

Kumar et al.

1 Tumors attenuating the mitochondrial activity in T cells escape from PD-1 blockade
2 therapy.

3

4 Alok Kumar*, Kenji Chamoto*, Partha S. Chowdhury, and Tasuku Honjo

5

6 Department of Immunology and Genomic Medicine, Graduate School of Medicine,
 7 Kyoto University, Kyoto, Japan.

8

9 Address correspondence to: Tasuku Honjo

10 Email: honjo@mfour.med.kyoto-u.ac.jp

11 Address: Department of Immunology and Genomic Medicine, Kyoto University,
 12 Graduate School of Medicine, Yoshida, Konoe-cho, Sakyo-ku, Kyoto, 606-8501, Japan.

13 Tel: +81-75-753-4371

14 Fax: +81-75-753-4388

15 *Equal contribution

16 Conflict of interest statement

17 The authors have declared that no conflict of interest exists.

18 **Keywords:** Cancer immunotherapy; Energy metabolism; Systemic immunosuppression;

19 Immune resistance; Oxygen consumption rate; Combination therapy;

Kumar et al.

20 **Abstract**

21 PD-1 blockade therapy has revolutionized cancer treatments. However, a
 22 substantial population of patients is unresponsive. To rescue unresponsive patients, the
 23 mechanism of unresponsiveness to PD-1 blockade therapy must be elucidated. Using a
 24 ‘bilateral tumor model’ where responsive and unresponsive tumors were inoculated into
 25 different sides of the mouse belly, we demonstrated that unresponsive tumors can be
 26 categorized into two groups: with and without systemic immunosuppressive property
 27 (SIP). The SIP-positive tumors released uncharacterized, non-proteinaceous small
 28 molecules which inhibited T cell proliferation and mitochondrial activation. By contrast,
 29 the SIP-negative B16 tumor, escaped from immunity by losing MHC class I expression.
 30 Unresponsiveness of SIP-positive tumors was partially overcome by improving the
 31 mitochondrial function with a mitochondrial activator; this was not successful to B16,
 32 which employs immune ignorance. These results demonstrated that our ‘bilateral tumor
 33 model’ was useful for stratifying tumors to investigate the mechanism of
 34 unresponsiveness and develop strategy for proper combination therapy.

Kumar et al.

35 **Introduction**

36 Cancer immunotherapy using immune checkpoint blockade, particularly
 37 antibodies against programmed cell death receptor 1 (PD-1) or its ligand (PD-L1), has
 38 made a revolution in cancer treatments as this treatment has durable response even to
 39 terminal stage cancers and lesser side-effects compared to the conventional cancer
 40 treatments (Brahmer et al., 2010; Couzin-Frankel, 2013; Hodi et al., 2010; Mahoney,
 41 Rennert, & Freeman, 2015; Topalian, Drake, & Pardoll, 2015). The success of clinical
 42 trials for the PD-1/PD-L1 axis blockade led the FDA to approve antibodies for PD-1 (e.g.
 43 nivolumab, pembrolizumab) or PD-L1 (e.g. Atezolizumab, Avelumab, Durvalumab) for
 44 different types of human cancers including metastatic non-small cell lung carcinoma
 45 (NSCLC), squamous cell lung cancer, renal cell carcinoma, Hodgkin's lymphoma, head
 46 and neck squamous cell carcinoma, and very recently, for microsatellite instability-high
 47 (MSI-H) or mismatch repair deficient (dMMR) cancers that include many late-stage
 48 cancers (Chowdhury, Chamoto, & Honjo, 2017).

49 Despite the impressive success rate of PD-1 blockade therapy, a significant
 50 fraction of patients is unresponsive. To further improve its efficacy, we must (i) identify
 51 biomarker(s) that predict the responsiveness/unresponsiveness and (ii) develop improved
 52 strategy including the combination therapy. For these improvements, we need to
 53 understand the mechanism of unresponsiveness to PD-1 blockade therapy. Most studies
 54 on biomarkers and resistance mechanisms have focused only on the tumor's intrinsic
 55 properties (Cristescu et al., 2018; Ribas, 2015; Rieth & Subramanian, 2018; Wellenstein
 56 & de Visser, 2018; Zou, Wolchok, & Chen, 2016). However, we need to elucidate the
 57 mechanism for unresponsiveness related to immune effector T cells to understand the

Kumar et al.

complicated interaction between cancer and immunity. Several studies have worked on the mechanism for unresponsiveness from the immunity side in different models. In one such model, the ‘Cold and Hot tumor hypothesis’, tumors can be roughly classified as ‘immunologically hot (inflamed)’ with an abundance of tumor infiltrating lymphocytes (TILs) and ‘immunologically cold (noninflamed)’ with an absence of a sufficient population of pre-existing immune cells (Bonaventura et al., 2019; van der Woude, Gorris, Halilovic, Figdor, & de Vries, 2017). In addition, some groups claim that clinical failures in many patients could be due to an imbalance between T-cell reinvigoration and tumor burden (Borcoman, Nandikolla, Long, Goel, & Tourneau, 2018; Huang et al., 2017).

CD8⁺ T cells, the major immune effector cells for attacking tumors, are subject to negative regulation by multiple mechanisms in tumor-bearing hosts. Some of the well-known negative regulatory cells and soluble factors include myeloid derived suppressor cells (MDSC), innate lymphoid cells (ILC), tumor associated macrophages (TAM), regulatory CD4 T cells (TReg), regulatory B cells (BReg), transforming growth factor β (TGF- β), interleukin-10 (IL-10), adenosine, granulocyte-macrophage colony-stimulating factor (GM-CSF), prostaglandin E2 (PGE2), and L-Kynurenine (Artis & Spits, 2015; DeNardo & Ruffell, 2019; Facciabene, Motz, & Coukos, 2012; Sarvaria, Madrigal, & Saudemont, 2017; Tauriello et al., 2018). Lack of MHC class I and neo-antigen on tumor cells also causes unresponsiveness because T cells cannot recognize the tumor (Garrido, Aptsiauri, Doorduijn, Garcia Lora, & van Hall, 2016; McGranahan et al., 2017; Rodriguez, 2017). The tumor microenvironment, influenced by the above mechanisms, allows tumor cells to escape from immune attack (DeNardo & Ruffell, 2019; Russo &

Kumar et al.

Protti, 2017). Due to this complexity of tumor and immunity interactions, it is difficult to determine which tumor employs which immune escape mechanism.

Energy metabolism mediated by mitochondrial activity regulates the fate of T cells. It has been reported that mitochondria play an important role in antigen-specific T cell activation through signaling of mitochondria-derived reactive-oxygen species (ROS) (Mallilankaraman, 2018; Murphy & Siegel, 2013; Sena et al., 2013). We recently reported that mitochondria are activated in tumor-reactive CTLs during PD-1 blockade therapy in MC38 tumor-bearing host (Chamoto et al., 2017). Boosting fatty acid oxidation with a metabolic modulator enhanced the PD-1 blockade effect (Chowdhury, Chamoto, Kumar, & Honjo, 2018). Therefore, attenuation of the mitochondrial activity of T cells by tumor-mediated factors could be an immune escape mechanism.

In this study, we developed a novel approach using a ‘bilateral tumor model’ and studied the immunosuppressive nature of unresponsive tumors to PD-1 blockade therapy. This model allowed us to categorize unresponsive tumors into two: those which have immune ignorance property and the others which have systemic immunosuppressive properties (SIP) by releasing factors to downregulate mitochondrial function and to inhibit T cell proliferation. Boosting the mitochondrial activity by the addition of bezafibrate, a pan-PPAR agonist, partially improved the efficacy of the PD-1 blockade against unresponsive tumors with SIP, but did not affect tumors introducing immune ignorance at the local site.

Kumar et al.

Results

Different immune responses between hosts with responsive and unresponsive tumors.

We first determined which tumor was responsive and unresponsive using the PD-1 blockade therapy model or the PD-1^{-/-} mouse model (Supplementary Figure S1). As summarized in Supplementary Table S1, MC38, GL261 and MethA were characterized as responsive tumors while LLC, Pan02, B16, and CT26 were characterized as unresponsive tumors.

Since CD8⁺ cytotoxic T lymphocytes (CTLs) are the main effector cells during PD-1 blockade therapy, we examined the difference in the immune responses to a responsive tumor and an unresponsive tumor according to the schedule shown in Figure 1A. We found both the total lymphocytes and the effector memory CD8⁺ T cells (defined as CD62L^{low} CD44^{high}, P3) in draining lymph nodes (DLNs) significantly increased in the group of responsive tumors, but did not change in unresponsive tumor-bearing hosts after PD-1 blockade (Figure 1B and C).

The frequency of CD8⁺ tumor-infiltrating lymphocytes (TILs) also increased after PD-1 blockade in the group of responsive tumor-bearing hosts, but not in unresponsive tumor-bearing hosts (Figure 1D). The expression of T-bet and IFN- γ , which reflect the activity of Th1-type cytotoxic activity, increased after PD-1 blockade treatment in the group bearing responsive tumors, but did not in the unresponsive tumor-bearing group (Figure 1E and F) (Sullivan, Juedes, Szabo, von Herrath, & Glimcher, 2003). Similar results were obtained in mice on another genetic background (BALB/c) (Supplementary

Kumar et al.

Figure S2). Taken together, anti-tumor immune responses increased only in hosts with responsive tumors but not in hosts with unresponsive tumors.

Higher mitochondrial activity of effector CD8⁺ T cells from mice with responsive tumors after PD-1 blockade

We and others have previously reported that mitochondrial activation in CD8⁺ T cells is a marker of CTL activation (Buck et al., 2016; Chamoto et al., 2017). Thus, to determine whether there was an association between the responsiveness to PD-1 blockade therapy and mitochondrial activation in T cells, we measured several markers of mitochondrial activation using the Seahorse Analyzer (Supplementary Figure S3A). We found that CD8⁺ T cells from responsive (MC38 and GL261) tumor-bearing hosts had significantly higher basal respiration, maximal respiration, spare respiratory capacity (SRC), and ATP turnover by PD-1 blockade, which was not observed in unresponsive (B16 and LLC) tumor-bearing hosts (Figure 2A). Similar results were obtained in mice on the BALB/c background (Supplementary Figure S3B). In addition, mitochondrial superoxide production (MitoSox) and Cellular ROS (CellRos) in CD8⁺ TIL were increased by PD-1 blockade therapy only in responsive tumor-bearing mice (Figure 2B and C). Together, increased activity in CD8⁺ T cells by PD-1 blockade in responsive tumor-bearing mice parallels with their activation status of mitochondria.

Classification of unresponsive tumors by the presence or absence of SIP

In order to investigate the mechanism of the systemic immune suppression of unresponsive tumors, we next employed a “bilateral tumor inoculation model” where unresponsive and responsive tumors were inoculated on different sides of the host (Figure 3A). This model facilitates disclosing how much humoral factors derived from

Kumar et al.

unresponsive tumors would contribute to the growth of responsive tumors in the other side. As shown in Figure 3B, we found that when unresponsive tumors (LLC or Pan02) were present on the left side, the growth inhibition of the responsive MC38 on the right by the PD-1 blockade therapy was inefficient. However, when the unresponsive B16 was on the left, the responsive MC38 or GL261 were rejected by PD-1 blockade as efficiently as the case in which no tumor was on the left side (Figure 3B and Supplementary Figure S4A). The sizes of the left unresponsive tumor in the same experiment were not inhibited by the PD-1 blockade therapy (Supplementary Figure S4B). Therefore, we speculated that the unresponsive LLC and Pan02 tumors may have released immune suppressive factors, while the unresponsive B16 did not.

Following the same experimental design, we performed the bilateral tumor experiment in mice on another background (BALB/c) and identified that CT26 is an unresponsive tumor with SIP (Figure 3C and Supplementary Figure S4C). Taken together, we classified unresponsive tumors into two groups: those with or without SIP (Table 1).

Tumor-derived suppressive soluble factor(s) systemically inhibits mitochondrial activity of CTLs *in vivo*

Since we observed mitochondrial activation in CD8⁺ T cells as a parameter of responsiveness (Figure 2), we used the bilateral tumor model to investigate how immunosuppressive factors released from unresponsive tumors (on the left side) inhibited the immune response against responsive tumors (on the right side) from the aspect of mitochondrial activation (Figure 4A). As shown in Figure 4B, the absolute number of lymphocytes in the DLN on the side with MC38 was increased by PD-1 blockade in mice

Kumar et al.

with the SIP-negative B16 on the other side, but not when the SIP-positive LLC was on the other side. Accordingly, mitochondrial ROS production, mass, OCR and ATP turnover in DLN CD8⁺ T cells were also enhanced by PD-1 blockade on the MC38 side in the presence of B16 on the other side, but not the case when SIP-positive LLC was inoculated on the other side (Figure 4C and D). In contrast, the PD-1 blockade treatment did not change the mitochondrial activation status in the unresponsive tumor sides (B16 and LLC) (Figure 4E and F). In summary, while both LLC and B16 were unresponsive, only the LLC systemically inhibited the mitochondrial activation of CTLs during the PD-1 blockade therapy.

The immunotherapy-resistant B16 tumor lacks MHC class I

We suspected that unresponsive tumors without SIP may not be recognized by acquired immunity. We compared tumor growth between wild type and immune-compromised mice (Rag2^{-/-}). As shown in Figure 5A, the growth of responsive tumors (MC38, GL261, and MethA) were significantly restricted in wild type compared with Rag2^{-/-} mice. In contrast, unresponsive tumors were more or less insensitive to acquired immunity (Figure 5B). Note that some unresponsive tumors with SIP (LLC and CT26) were sensed to a small extent by acquired immunity while unresponsive tumors without SIP (B16) were completely ignored (Table 1). This complete ignorance could be attributed to deficiencies in the “T cell - tumor cell interaction” probably due to less neoantigen and/or lack of MHC class I expression. Indeed, we found that B16 does not express MHC class I even after stimulation with IFN- γ , but others do (Figure 5C and D).

These data indicate that one of the mechanisms of unresponsiveness in tumors without SIP is lack of MHC class I expression, and suggest that elimination of the

Kumar et al.

suppressive factor would facilitate enhancement of PD-1 blockade therapeutic efficacy only in unresponsive tumors with SIP.

Secretion of immune inhibitory small molecules from SIP-positive tumors

To examine whether immune suppressive factors are released from unresponsive tumors, naïve CD8⁺ T cells were stimulated with anti-(CD3+CD28) mAb-coated beads in the presence of supernatants collected from responsive and unresponsive tumor cell cultures (Figure 6A). Proliferation assays (thymidine incorporation and Ki67 detection assays) demonstrated that T cell proliferation was significantly inhibited in the presence of supernatants from LLC or CT26, but not in the presence of supernatants from B16, GL261 or MethA (Figure 6B and Supplementary Figure S5A and B). The suppressive effects of soluble factors from the LLC supernatant was further evidenced by restoration of T cell proliferation when the supernatant was diluted (Supplementary Figure S5C).

In addition, different parameters of mitochondrial activation such as cellular ROS and mitochondrial potential were significantly inhibited by the LLC supernatant compared with the B16 and GL261 supernatants (Figure 6C). The OCR and the extracellular acidification rate (ECAR), a parameter for glycolytic function, were severely reduced in CD8⁺ T cells cultured for 48 hours in the presence of LLC supernatants compared with those from B16 and GL261 (Figure 6D and E). Similar suppressive activities were observed by supernatants from BALB/c background tumor CT26 (Supplementary Figure S5D). These results indicate that the immunosuppressive factors released from SIP-positive tumors inhibit the mitochondrial function and proliferation of CD8⁺ T cells.

Kumar et al.

In order to understand the molecular properties of suppressive factors, we performed heat-inactivation to denature protein components and used a dextran-coated charcoal treatment (DCC) to adsorb small molecules in the culture supernatants. As shown in Figure 6F and Supplementary Figure S5E, heat-inactivation of LLC and CT26 culture supernatants did not abolish their suppressive activity, whereas removing low molecular weight compounds using the DCC treatment eliminated their suppressive activity, suggesting that the suppressive factor(s) may be comprised of non-proteinaceous small molecules. We further fractionated the supernatant into ‘Fraction A (< 3 KDa)’ and ‘Fraction B (3~50 KDa)’ and found that Fraction A had almost the same inhibition potential as the total culture supernatants (Figure 6G and Supplementary Figure S5F). Again, removing small molecules from Fraction A using the DCC treatment restored the proliferation of CD8⁺ T cells.

Since the tumor-derived soluble suppressive factor(s) are small, non-protein molecules with a size less than 3 kDa, we tested whether known candidates such as adenosine, Prostaglandin E2 (PGE₂) and kynurenine show similar activities. However, the suppressive tumors did not express the significant level of related enzymes including CD39, CD73, COX-2, mPGES1 and IDO (Supplementary Figure S6).

Combination of bezafibrate with PD-1 blockade improves survival of mice bearing SIP-positive tumors

Since SIP reduced the mitochondrial activity, we examined whether mitochondria activation drug combination can reverse the immune suppression by SIP-positive tumors. As bezafibrate activates mitochondria and synergizes with PD-1 blockade therapy, we first tested whether bezafibrate can reverse the suppression of mitochondrial function and

Kumar et al.

237 proliferation caused by suppressive factors from the LLC culture supernatants *in vitro*
 238 (Chowdhury et al., 2018). Proliferation and mitochondrial function were regained
 239 significantly when bezafibrate was used along with culture supernatant (Figure 7A).
 240 Encouraged with these *in vitro* results, we performed PD-1 blockade combinatorial
 241 therapy with bezafibrate for LLC tumor-bearing hosts (Figure 7B). We found that the
 242 tumor-killing effect by the PD-1 blockade was enhanced and mouse survival was
 243 increased in the combination therapy (Figure 7C). Of note is the fact that the
 244 combinatorial treatment could not rescue the B16-bearing host (Figure 7C). We observed
 245 similar results in tumors on the BALB/c background. The survival of SIP-positive CT26-
 246 bearing hosts was improved with the combinatorial therapy with bezafibrate
 247 (Supplementary Figure S7). In summary, the SIP effects of unresponsive tumors were
 248 partially rescued by a mitochondrial activation chemical, bezafibrate *in vitro* and *in vivo*.

Kumar et al.

249 Discussion

250 One of the biggest issues in PD-1 blockade cancer immunotherapy is how to
 251 reduce the rate of unresponsiveness. Although there are many unresponsive mechanisms,
 252 cancers employ at least two strategies to escape from the immune attack: local or
 253 systemic immune suppression. Some reports have suggested “hot tumors” and “cold
 254 tumors” to distinguish responsive and unresponsive tumors based on the level of immune
 255 cell infiltration in the tumor mass (van der Woude et al., 2017). However, it is difficult to
 256 explain molecular mechanisms of unresponsiveness by this definition because it explains
 257 the results of immune responses in local tumor areas, but not the induction phase of
 258 immune escape.

259 In this paper, we employed the bilateral tumor inoculation model, which can
 260 distinguish local immune suppression including ignorance from systemic immune
 261 suppression *in vivo*, and categorized unresponsive tumors into two groups, with or
 262 without SIP. Small molecules with less than 3 kDa size which is released from SIP-
 263 positive tumors appear to attenuate mitochondria-mediated energy metabolism in T cells.
 264 We rule out the known factors such as suppressive cytokines, adenosine, Prostaglandin
 265 E2 (PGE₂) and kynurenine. Tumor cells show dysregulated cellular metabolism and the
 266 metabolic products often induce immune suppression (Deberardinis, 2008; Munn &
 267 Mellor, 2013; Vazquez et al., 2016). Although it has been reported that methyl-
 268 nicotinamide (MNA), which is converted by nicotinamide N-methyl-transferase
 269 (NNMT), acts as an immune suppressive factor (Gebicki et al., 2003), this compound
 270 showed no suppression at physiological levels (data not shown). Other metabolites could
 271 be candidates, which are derived from tumor’s metabolic activity.

Kumar et al.

For successful PD-1 blockade therapy, the “tumor-immunity cycle” needs to operate smoothly (Chen & Mellman, 2013; Pio, Ajona, Ortiz-Espinosa, Mantovani, & Lambris, 2019). Hindrance in the pathway at any steps of antigen recognition, activation, recruitment and killing at the tumor site, DLN or blood stream would lead to the unresponsive state (Mushtaq et al., 2018). DLN is generally considered as a place where naïve T cells are primed to effector T cells. Our bilateral model analysis suggests that LLC systemically inhibits T cell priming at DLN of responsive tumor sides via suppressive factors, but B16 does not. However, it seems contradict that T cells in DLN on the side of B16 was not activated in spite of the deficiency of SIP. This observation suggests that tumor recognition by the local tumor area is critical to trigger T cell priming in DLN and to establish the successful tumor-immunity cycle. Therefore, tumors lacking MHC take advantage of the ignorance or escape mechanism not only in the local tumor area, but also in DLN. Given that LLC expresses MHC and is sensitive to the acquired immunity to some extent, it is reasonable that LLC but not B16 is susceptible to the combination therapy.

Mitochondrial activation is essential for full activation of T cells. In our *in vitro* assay system for mitochondrial activities, we stimulated naïve CD8⁺ T cells by anti-(CD3+CD28) mAb beads because CD28 in addition to CD3 signal is necessary for robust mitochondria during the proliferation (Klein Geltink et al., 2017). Although our OCR data suggest that the suppressive factor downregulates the mitochondrial activity, ECAR also severely inhibited. Therefore, the suppressive factor may inhibit the glycolysis, resulting in the attenuation of subsequent OXPHOS reactions. This hypothesis agrees with the fact that T cells rely on glycolysis more than OXPHOS when they differentiate

Kumar et al.

from naïve to effector T cells (Menk et al., 2018). Another possible mechanism for suppression of mitochondrial function by the suppressive factors is inhibition of the downstream signals of CD3 and/or CD28 because these 2 signals are necessary for upregulation of glycolysis and OXPHOS in T cells.

In this work, we applied bezafibrate to unresponsive LLC or CT26 tumors. We found this combination therapy partially restored the PD-1 blockade effect in accordance with the *in vitro* assays where bezafibrate partially removed the mitochondrial inhibition by the suppressive factors in the supernatant. This partial effect suggests that under the situation of “brake” induced by the suppressive factors, the “acceleration” by PGC-1 α /PPAR activation would not fully work. In order to obtain the maximum benefit, we need to define the suppressive factors and remove the “brake”. Our data suggest the possibility of unknown small molecules for suppressive factors. Purification of this small molecule by bio-assays will enable us to identify its structure by mass spectrometry. Once we know such compound, we may be able to find the enzymes responsible for the synthesis of this product and target them for combinatorial treatment.

310

Kumar et al.

Methods

Animals

C57BL/6N and BALB/c inbred mice were purchased from ‘The Charles River Laboratories, Japan (Kanagawa, Japan)’. PD-1^{-/-} and RAG2^{-/-} inbred mice lines were maintained under specific pathogen-free conditions at the Institute of Laboratory Animals, Graduate School of Medicine, Kyoto University. Female, 6-8 weeks-old mice were used in all the experiments.

Cell culture

Cell lines were cultured in RPMI or DMEM medium (Gibco, Grand Island, NY, USA; catalog #11875-093 and 11995-065 respectively) with 10% (v/v) heat-inactivated fetal bovine serum and 1% (v/v) penicillin-streptomycin mixed solution (Nacalai Tesque, Kyoto, Japan, 26253-84) as per the instructions recommended by the ATCC. Cell lines were free of *mycoplasma* contamination. Cell cultures were maintained at 37 °C with 5% CO₂ in a humidified incubator. Details of different cell lines used in the experiment e.g. source of cell lines, background and origin of cancer, etc. are mentioned in Supplementary Table S1. The tumor cell lines MethA and GL261 were passaged *in vivo* once before use in experiments.

Monotherapy model using anti-PD-L1 antibody

Tumor cells were intradermally (i.d.) injected into the right flank of mice (day 0). Monotherapy with the anti-PD-L1 antibody was started when the tumor size reached 50–60 mm³ (around day 5). Mice were intraperitoneally (i.p.) injected with 80 µg of anti-PD-L1 mAb (clone 1-111A.4); mAb injection was repeated every fifth day. For untreated

Kumar et al.

mice, an isotype control for the anti-PD-L1 mAb (Rat IgG2a, κ) was injected. Tumor sizes were measured every alternate day using a digimatic caliper (Mitutoyo Europe GmbH, Germany) and tumor volume was calculated using the formula for a typical ellipsoid [$\pi \times (\text{length} \times \text{breadth} \times \text{height})/6$].

Bilateral tumor model

First, unresponsive tumor cells were i.d.- injected into the left flank of mice (day 0). When the size of the unresponsive tumor was around 60-70 mm³ (around day 6-7), responsive tumor cells were i.d.- injected into the right flank. Two-three days after the responsive tumor injection (around day 9-10), anti-PD-L1 antibody was injected following a monotherapy treatment model (for the dose of antibody and interval between two injections). Tumor sizes of responsive and unresponsive tumors were measured every alternate day and tumor volume was calculated according the formula mentioned earlier.

Chemical reagents

Bezafibrate (Santa Cruz Biotechnology, Dallas, TX, USA) was used at the dose of 5 mg/kg for *in vivo* combination therapy. Bezafibrate was freshly prepared, immediately before use, in DMSO. Dissolved bezafibrate was diluted in PBS and 200 μ L was i.p.- injected per mouse. Bezafibrate was added at the concentration of 5 μ M for *in vitro* assays throughout this work wherever it is used, unless specified.

Combination therapy model

For combination therapy experiments, the therapy started when the tumor size was 60-70 mm³. Mice were i.p.- injected with 40 μ g of anti-PD-L1 mAb (clone 1-111A.4); the mAb injection was repeated every sixth day. Mice were i.p.-injected with bezafibrate at 5 mg/kg dose every third day. For control groups, an isotype control for the

Kumar et al.

anti-PD-L1 mAb (Rat IgG2a, κ) and DMSO vehicle for bezafibrate were injected. All groups were subjected to the same dose of DMSO. Tumor measurement was performed as stated above.

Naïve CD8⁺ T cell isolation

To isolate naïve CD8⁺ T cells from C57BL/6N inbred wild-type mice, the spleen and three LNs (axillary, brachial, and inguinal LNs) from both the right and left sides were harvested. The spleen was minced, treated with ACK lysis buffer (0.15 M NH₄Cl + 1.0 mM KHCO₃ + 0.1 mM Na₂-EDTA) for 2 min to lyse the erythrocytes, and mixed with pooled and minced LN cells. Naïve (CD62L^{high} CD44^{low}) CD8⁺ T cells were then purified from total pooled lymphocytes according to the manufacturer's instructions (Miltenyi Biotec, 130-096-543). For *in vitro* analysis, naïve CD8⁺ T cells were stimulated with anti-CD3 and CD28 mAb-coated dynabeads (Thermo Fisher Scientific, Gibco, Catalog# 11452D).

Collection of culture supernatants from different cell lines

We seeded 0.5 million cells/well in 6-well plates in 4 mL total volume of respective media as recommended by the ATCC. After 48 hours of incubation, we harvested the culture supernatant, centrifuged at 10000 x g for 15 minutes at 22 °C, collected the supernatant, and kept it at -80 °C for storage. We added culture supernatant one-fourth of the total volume in the well (96-well round bottom plate) throughout the *in vitro* assays with naïve CD8⁺ T cells in this work, unless specified.

Thymidine incorporation assay

Thymidine solution diluted in spleen RPMI (Basal RPMI media with 10% FCS, 1% Penicillin-Streptomycin, 50 μ M 2-Mercapto ethanol, L-Glutamine, Na-pyruvate,

Kumar et al.

NEAA) was added to cells and incubated for 4 hours at 37 °C in a humidified incubator with 5% CO₂. After incubation, cells were transferred to a 96-well filter plate followed by addition of scintillation buffer. Thymidine uptake was measured on a Microbeta² microplate counter (PerkinElmer, # 2450-0120) machine.

Heat-inactivation treatment of supernatant:

To inactivate the protein component, culture supernatant was boiled for 10 minutes at 95 °C followed by centrifugation at 10,000 x g for 30 minutes. The supernatant was collected and stored at -80 °C for storage.

Dextran-coated charcoal (DCC) treatment of supernatant:

To remove small molecules, the supernatant was treated with DCC, which removes small molecules (e.g. nucleotides, vitamins, lipids) from the sample by adsorbing them on the surface. To remove small molecules, 12 mg DCC (for 500 µL supernatant) was added and incubated for 20 min at 25 °C, followed by centrifugation at 10,000 x g for 30 minutes. After centrifugation, the supernatant that was free from small molecules was collected.

Fractionation of culture supernatant

Cultures supernatants were fractionated into different fractions using amicon ultra-centrifugal filters (Merck Millipore Ltd., Ireland) with cut-off sizes of 3KDa and 50KDa. Supernatants were added to 3KDa filter and centrifuged at 12000 x g for 30 minutes at 4 °C. The filtered supernatant was collected and further fractionated using higher cut-off filter (50KDa) in similar way.

Cell preparation for analysis

For draining lymph node (DLN) analysis, axillary, brachial, and inguinal LNs

Kumar et al.

(one of each) were harvested from the tumor-bearing side (left or right flank) of mice. All LNs were minced and pooled. Average LN cell numbers (total pooled LN cells/3) were used as absolute cell numbers. For tumor-infiltrating lymphocyte (TIL) analysis, tumor tissue was harvested and cut into 1–2 mm pieces with scissors followed by digestion with collagenase type IV (Worthington Biochemical Corporation, Lakewood, NJ, Catalog # LS004188) using a gentle MACS Dissociator (Miltenyi Biotec). The numbers of TILs per mg of tumor tissue were used as the absolute numbers.

Flow cytometry analysis

The following monoclonal antibodies (mAbs) were used to detect the respective antigens during FACS staining: CD8 (53-6.7), CD62L (MEL-14), CD44 (IM7), CD45.2 (104), T-bet (4B10), IFN- γ (XMG-1.2) from BioLegend (San Diego, CA, USA); and Ki67 (SolA15) from eBioscience (San Diego, CA, USA). All flow cytometry experiments were performed on a FACS Canto II (BD Biosciences, Franklin Lakes, NJ, USA), and analyzed using the FlowJo software (FLOWJO, LLC, Ashland, OR, USA).

Mitochondrial mass, membrane potential, mitochondrial superoxide, and cellular ROS were determined by MitoTracker Green, MitoTracker Deep Red, MitoSOX Red, and CellROX Green reagents, respectively (all from Life Technologies, Carlsbad, CA, USA). The cells were washed twice with D-PBS buffer followed by the addition of dye solution with final concentrations of 0.125, 0.125, 5.0, and 0.625 μ M, respectively, in RPMI media and incubated at 37 °C in a 5% CO₂ humidified incubator for 30 min. After incubation, cells were washed twice with D-PBS buffer followed by surface staining.

Intranuclear staining

For intranuclear staining, cells were fixed and permeabilized using Foxp3 staining

Kumar et al.

kit (Thermo Fisher scientific, Catalog # 00-5523-00) following the manufacturer's instructions. After fixation and permeabilization, cells were incubated with the respective antibody for 15 minutes at 4 °C in the dark, followed by washing with FACS buffer (PBS, 0.5-1% BSA or 5-10% FBS, 0.1% NaN₃ sodium azide).

Intracellular cytokine staining for IFN- γ

Homogenized tumor mass cells from *in vivo* treated experimental mice were incubated for 4 hours at 37 °C in a 5% CO₂ humidified incubator. After incubation, Brefeldin A and Monensin (eBioscience, Invitrogen, Carlsbad, CA, USA; catalog # 4506-51 and 4505-51 respectively) were added at the concentration of 5 µg/mL and 2 µM as per the manufacturer's instructions and incubated for further 2 hours. Following a total of six hours of incubation, cells were washed once with D-PBS and further stained for surface proteins, if any. Cells were then fixed with 1.5% paraformaldehyde solution (incubated for 15 minutes at 4 °C) and washed twice with FACS buffer. Cells were then treated with 0.5% Triton-X-100 in PBS and incubated for 15 minutes at 4 °C to permeabilize the cells. Monoclonal antibodies to IFN- γ were added (the concentration was pre-optimized) and incubated for 15 minutes at 4 °C followed by washing with FACS buffer.

Real-time RT-PCR

We isolated RNA from different cancer cell lines with the RNeasy mini kit (QIAGEN, Hilden, Germany) and synthesized cDNA by reverse transcription (Invitrogen). The primers used to perform real-time PCR are listed in Supplementary Table S2.

Measurement of oxygen consumption rates and extracellular acidification rate

Kumar et al.

448 The oxygen consumption rate (OCR) and extracellular acidification rate (ECAR)
 449 of treated cells were measured using an XF[®]96 Extracellular Flux analyzer (Seahorse
 450 Biosciences, North Billerica, MA, USA). One day before the experiment, first the XF[®]96
 451 plate was coated with CellTak solution as per the manufacturer's recommendation. On
 452 the day of experiment, all chemicals (e.g. Oligomycin, FCCP and Rotenone/Antimycin
 453 A) were prepared in OCR media as per the manufacturer's recommendation and the
 454 machine was calibrated using the calibrant buffer in the calibrant plate prior to the
 455 experiment. 400 thousand cells per well were seeded in the precoated XF[®]96 plate and the
 456 OCR/ECAR was measured. Different parameters from the OCR graph were calculated.
 457 ATP turnover was defined as follows: (last rate measurement before oligomycin) -
 458 (minimum rate measurement after oligomycin injection). Maximal respiration was
 459 defined as follows: (maximum rate measurement after FCCP) - (non-mitochondrial
 460 respiration). Spare respiratory capacity (SRC) was calculated by subtracting basal
 461 respiration from maximal respiration. We measured the ECAR value in the same well,
 462 which contained an optimal glucose level so the basal ECAR (or glycolysis) value is the
 463 reading we obtained immediately before oligomycin injection. We prepared the assay
 464 medium as described in the XF cell Mito Stress Test Kit (Kit 103015-100). The glucose
 465 concentration in this medium is 10 mM. In the classical glycolytic assay procedure
 466 (glucose-free media) the final concentration of glucose added to the port was 10 mM
 467 while measuring flux. The basal ECAR value in this classical method is calculated by
 468 subtracting the last rate measurement before the glucose injection from the maximum rate
 469 measurement before the oligomycin injection, which gives essentially the same value if
 470 calculated by our method. Glycolytic capacity was defined as the rate measured after the

Kumar et al.

oligomycin injection. The glycolytic reserve was defined as follows: (glycolytic capacity)
– (basal ECAR value).

Statistics

Statistical analysis was performed using Prism 6 (GraphPad Software, La Jolla, CA, USA). One-way ANOVA analysis followed by Sidak's multiple comparison test was utilized to analyze three or more variables. To compare two groups, student *t* test was used. All statistical tests were two-sided assuming parametric data, and a *p* value of < 0.05 was considered significant. The variations of data were evaluated as the means ± standard error of the mean (SEM). Five or more samples were thought to be appropriate for the sample size estimate in this study. Samples and animals were randomly chosen from the pool and treated. No blinding test was used for the treatment of samples and animals.

Study approval

Mice were maintained under specific pathogen-free conditions at the Institute of Laboratory Animals, Graduate School of Medicine, Kyoto University under the direction of the Institutional Review Board.

Kumar et al.

Author Contributions

Conception and design: K. Chamoto, T. Honjo

Development of methodology: A. Kumar, K. Chamoto

Acquisition of data (provided animals, acquired and managed patients, provided facilities, etc.): A. Kumar, P.S. Chowdhury, K. Chamoto

Analysis and interpretation of data (e.g., statistical analysis, biostatistics, computational analysis): A. Kumar, P.S. Chowdhury, K. Chamoto

Writing, review, and/or revision of the manuscript: A. Kumar, K. Chamoto, T. Honjo

Study supervision: A. Kumar, P.S. Chowdhury, T. Honjo

Acknowledgments

We thank M. Al-Habsi, M. Akrami, T. Oura, R. Hatae, Y. Nakajima, R. M. Menzes, K. Yurimoto and Y Kitawaki for assistance in sample preparation;

Financial support: This work was supported by AMED under grant number of JP19cm0106302, JP19gm0710012 (TH), and JP191k1403006 (KC); Tang Prize Foundation (TH); JSPS KAKENHI Grant number JP16H06149, 17K19593 (KC), 17F17119 (PSC), 18J15051(AK); the Cell Science Foundation (KC).

References

- Artis, D., & Spits, H. (2015). The biology of innate lymphoid cells. *Nature*, 517(7534), 293-301. doi:10.1038/nature14189
- Bonaventura, P., Shekarian, T., Alcazer, V., Valladeau-Guilemond, J., Valsesia-Wittmann, S., Amigorena, S., . . . Depil, S. (2019). Cold Tumors: A Therapeutic Challenge for Immunotherapy. *Frontiers in Immunology*, 10(168). doi:10.3389/fimmu.2019.00168
- Borcoman, E., Nandikolla, A., Long, G., Goel, S., & Tourneau, C. L. (2018). Patterns of Response and Progression to Immunotherapy. *American Society of Clinical Oncology Educational Book*(38), 169-178. doi:10.1200/edbk_200643
- Brahmer, J. R., Drake, C. G., Wollner, I., Powderly, J. D., Picus, J., Sharfman, W. H., . . . Topalian, S. L. (2010). Phase I study of single-agent anti-programmed death-1 (MDX-1106) in refractory solid tumors: safety, clinical activity, pharmacodynamics, and immunologic correlates. *J Clin Oncol*, 28(19), 3167-3175. doi:10.1200/JCO.2009.26.7609
- Buck, M. D., O'Sullivan, D., Klein Geltink, R. I., Curtis, J. D., Chang, C. H., Sanin, D. E., . . . Pearce, E. L. (2016). Mitochondrial Dynamics Controls T Cell Fate through Metabolic Programming. *Cell*, 166(1), 63-76. doi:10.1016/j.cell.2016.05.035
- Chamoto, K., Chowdhury, P. S., Kumar, A., Sonomura, K., Matsuda, F., Fagarasan, S., & Honjo, T. (2017). Mitochondrial activation chemicals synergize with surface receptor PD-1 blockade for T cell-dependent antitumor activity. *Proc Natl Acad Sci U S A*, 114(5), E761-e770. doi:10.1073/pnas.1620433114
- Chen, D. S., & Mellman, I. (2013). Oncology meets immunology: the cancer-immunity cycle. *Immunity*, 39(1), 1-10. doi:10.1016/j.immuni.2013.07.012
- Chowdhury, P. S., Chamoto, K., & Honjo, T. (2017). Combination therapy strategies for improving PD-1 blockade efficacy: a new era in cancer immunotherapy. *J Intern Med*. doi:10.1111/joim.12708
- Chowdhury, P. S., Chamoto, K., Kumar, A., & Honjo, T. (2018). PPAR-Induced Fatty Acid Oxidation in T Cells Increases the Number of Tumor-Reactive CD8(+) T Cells and Facilitates Anti-PD-1 Therapy. *Cancer Immunol Res*, 6(11), 1375-1387. doi:10.1158/2326-6066.Cir-18-0095
- Couzin-Frankel, J. (2013). Breakthrough of the year 2013. Cancer immunotherapy. *Science*, 342(6165), 1432-1433. doi:10.1126/science.342.6165.1432
- Cristescu, R., Mogg, R., Ayers, M., Albright, A., Murphy, E., Yearley, J., . . . Kaufman, D. (2018). Pan-tumor genomic biomarkers for PD-1 checkpoint blockade-based immunotherapy. *Science*, 362(6411). doi:10.1126/science.aar3593
- Deberardinis, R. J. (2008). Is cancer a disease of abnormal cellular metabolism? New angles on an old idea. *Genetics In Medicine*, 10, 767. doi:10.1097/GIM.0b013e31818b0d9b
- DeNardo, D. G., & Ruffell, B. (2019). Macrophages as regulators of tumour immunity and immunotherapy. *Nat Rev Immunol*, 19(6), 369-382. doi:10.1038/s41577-019-0127-6

Kumar et al.

- 553 Facciabene, A., Motz, G. T., & Coukos, G. (2012). T-regulatory cells: key players in
554 tumor immune escape and angiogenesis. *Cancer Res*, 72(9), 2162-2171.
555 doi:10.1158/0008-5472.Can-11-3687
- 556 Garrido, F., Aptsiauri, N., Doorduijn, E. M., Garcia Lora, A. M., & van Hall, T. (2016).
557 The urgent need to recover MHC class I in cancers for effective immunotherapy.
558 *Current opinion in immunology*, 39, 44-51. doi:10.1016/j.coi.2015.12.007
- 559 Gebicki, J., Sysa-Jedrzejowska, A., Adamus, J., Wozniacka, A., Rybak, M., & Zielonka,
560 J. (2003). 1-Methylnicotinamide: a potent anti-inflammatory agent of vitamin
561 origin. *Pol J Pharmacol*, 55(1), 109-112.
- 562 Hodi, F. S., O'Day, S. J., McDermott, D. F., Weber, R. W., Sosman, J. A., Haanen, J.
563 B., . . . Urban, W. J. (2010). Improved survival with ipilimumab in patients with
564 metastatic melanoma. *N Engl J Med*, 363(8), 711-723.
565 doi:10.1056/NEJMoa1003466
- 566 Huang, A. C., Postow, M. A., Orlowski, R. J., Mick, R., Bengsch, B., Manne, S., . . .
567 Wherry, E. J. (2017). T-cell invigoration to tumour burden ratio associated with
568 anti-PD-1 response. *Nature*, 545(7652), 60-65. doi:10.1038/nature22079
- 569 Klein Geltink, R. I., O'Sullivan, D., Corrado, M., Bremser, A., Buck, M. D., Buescher, J.
570 M., . . . Pearce, E. L. (2017). Mitochondrial Priming by CD28. *Cell*, 171(2), 385-
571 397.e311. doi:https://doi.org/10.1016/j.cell.2017.08.018
- 572 Mahoney, K. M., Rennert, P. D., & Freeman, G. J. (2015). Combination cancer
573 immunotherapy and new immunomodulatory targets. *Nat Rev Drug Discov*, 14(8),
574 561-584. doi:10.1038/nrd4591
- 575 Mallilankaraman, K. B. (2018). Chapter 5 - Mitochondrial ROS and T Cell Activation. In
576 S. Chatterjee, W. Jungraithmayr, & D. Bagchi (Eds.), *Immunity and Inflammation*
577 *in Health and Disease* (pp. 57-64): Academic Press.
- 578 McGranahan, N., Rosenthal, R., Hiley, C. T., Rowan, A. J., Watkins, T. B. K., Wilson, G.
579 A., . . . Dessimoz, C. (2017). Allele-Specific HLA Loss and Immune Escape in
580 Lung Cancer Evolution. *Cell*, 171(6), 1259-1271.e1211.
581 doi:https://doi.org/10.1016/j.cell.2017.10.001
- 582 Menk, A. V., Scharping, N. E., Moreci, R. S., Zeng, X., Guy, C., Salvatore, S., . . .
583 Delgoffe, G. M. (2018). Early TCR Signaling Induces Rapid Aerobic Glycolysis
584 Enabling Distinct Acute T Cell Effector Functions. *Cell Rep*, 22(6), 1509-1521.
585 doi:10.1016/j.celrep.2018.01.040
- 586 Munn, D. H., & Mellor, A. L. (2013). Indoleamine 2,3 dioxygenase and metabolic
587 control of immune responses. *Trends Immunol*, 34(3), 137-143.
588 doi:10.1016/j.it.2012.10.001
- 589 Murphy, M. P., & Siegel, R. M. (2013). Mitochondrial ROS fire up T cell activation.
590 *Immunity*, 38(2), 201-202. doi:10.1016/j.immuni.2013.02.005
- 591 Mushtaq, M. U., Papadas, A., Pagenkopf, A., Flietner, E., Morrow, Z., Chaudhary, S. G.,
592 & Asimakopoulou, F. (2018). Tumor matrix remodeling and novel
593 immunotherapies: the promise of matrix-derived immune biomarkers. *Journal for*
594 *ImmunoTherapy of Cancer*, 6(1), 65. doi:10.1186/s40425-018-0376-0
- 595 Pio, R., Ajona, D., Ortiz-Espinosa, S., Mantovani, A., & Lambris, J. D. (2019).
596 Complementing the Cancer-Immunity Cycle. *Front Immunol*, 10, 774.
597 doi:10.3389/fimmu.2019.00774

Kumar et al.

- 598 Ribas, A. (2015). Adaptive Immune Resistance: How Cancer Protects from Immune
599 Attack. *Cancer discovery*, 5(9), 915-919. doi:10.1158/2159-8290.CD-15-0563
- 600 Rieth, J., & Subramanian, S. (2018). Mechanisms of Intrinsic Tumor Resistance to
601 Immunotherapy. *International journal of molecular sciences*, 19(5), 1340.
602 doi:10.3390/ijms19051340
- 603 Rodriguez, J. A. (2017). HLA-mediated tumor escape mechanisms that may impair
604 immunotherapy clinical outcomes via T-cell activation. *Oncol Lett*, 14(4), 4415-
605 4427. doi:10.3892/ol.2017.6784
- 606 Russo, V., & Protti, M. P. (2017). Tumor-derived factors affecting immune cells.
607 *Cytokine Growth Factor Rev*, 36, 79-87. doi:10.1016/j.cytogfr.2017.06.005
- 608 Sarvaria, A., Madrigal, J. A., & Saudemont, A. (2017). B cell regulation in cancer and
609 anti-tumor immunity. *Cell Mol Immunol*, 14(8), 662-674.
610 doi:10.1038/cmi.2017.35
- 611 Sena, L. A., Li, S., Jairaman, A., Prakriya, M., Ezponda, T., Hildeman, D. A., . . .
612 Chandel, N. S. (2013). Mitochondria are required for antigen-specific T cell
613 activation through reactive oxygen species signaling. *Immunity*, 38(2), 225-236.
614 doi:10.1016/j.immuni.2012.10.020
- 615 Sullivan, B. M., Juedes, A., Szabo, S. J., von Herrath, M., & Glimcher, L. H. (2003).
616 Antigen-driven effector CD8 T cell function regulated by T-bet. *Proc Natl Acad
617 Sci U S A*, 100(26), 15818-15823. doi:10.1073/pnas.2636938100
- 618 Tauriello, D. V. F., Palomo-Ponce, S., Stork, D., Berenguer-Llargo, A., Badia-Ramentol,
619 J., Iglesias, M., . . . Batlle, E. (2018). TGFbeta drives immune evasion in
620 genetically reconstituted colon cancer metastasis. *Nature*, 554(7693), 538-543.
621 doi:10.1038/nature25492
- 622 Topalian, S. L., Drake, C. G., & Pardoll, D. M. (2015). Immune checkpoint blockade: a
623 common denominator approach to cancer therapy. *Cancer Cell*, 27(4), 450-461.
624 doi:10.1016/j.ccell.2015.03.001
- 625 van der Woude, L. L., Gorris, M. A. J., Halilovic, A., Figdor, C. G., & de Vries, I. J. M.
626 (2017). Migrating into the Tumor: a Roadmap for T Cells. *Trends Cancer*, 3(11),
627 797-808. doi:10.1016/j.trecan.2017.09.006
- 628 Vazquez, A., Kamphorst, J. J., Markert, E. K., Schug, Z. T., Tardito, S., & Gottlieb, E.
629 (2016). Cancer metabolism at a glance. *Journal of Cell Science*, 129(18), 3367.
630 doi:10.1242/jcs.181016
- 631 Wellenstein, M. D., & de Visser, K. E. (2018). Cancer-Cell-Intrinsic Mechanisms
632 Shaping the Tumor Immune Landscape. *Immunity*, 48(3), 399-416.
633 doi:https://doi.org/10.1016/j.immuni.2018.03.004
- 634 Zou, W., Wolchok, J. D., & Chen, L. (2016). PD-L1 (B7-H1) and PD-1 pathway
635 blockade for cancer therapy: Mechanisms, response biomarkers, and
636 combinations. *Sci Transl Med*, 8(328), 328rv324.
637 doi:10.1126/scitranslmed.aad7118
- 638

639

Kumar et al.

Figure Legends

Figure 1: PD-1 blockade significantly enhances the number and function of effector CD8⁺ T cells in mice with responsive, but not in those with unresponsive tumors.

(A) Schematic diagram of the experimental schedule. (B) Absolute number of lymphocytes per lymph node were calculated and compared among mice with different responsive or unresponsive tumors. (C) DLN cells were stained with anti-CD8, anti-CD62L, and anti-CD44 antibodies. Representative FACS patterns after gating on CD8⁺ T cells in each group with or without PD-1 blockade (top panel). Schematic representation of subpopulations among CD8⁺ T cells (bottom panel, left). Bar graphs of frequency and absolute number of effector memory (CD62L^{low} CD44^{high}; P3, hereinafter) population are shown (bottom panel, middle and right). (D) Cells after tumor digestion were stained with anti-CD8, and anti-CD45.2 antibodies. CD45.2⁺ CD8⁺ TIL frequency was compared between control IgG and anti-PD-L1 treated groups in responsive and unresponsive tumor-bearing hosts. Representative FACS pattern (upper panel) and the respective bar graph (lower panel) of CD45.2⁺ CD8⁺ TIL frequency are shown. (E) Harvested tumor mass cells from experimental groups were stained with anti-CD8, anti-CD45.2, and anti-T-bet antibodies. T-bet expression was plotted after gating on CD45.2⁺ CD8⁺ T cells. Representative FACS pattern from GL261 group (ctrl IgG treated) is shown (left). The frequency of T-bet among CD45.2⁺ CD8⁺ TILs of mice with different tumor are shown. (F) IFN- γ expression was intracellularly analyzed in the same way as (E). Representative FACS pattern from GL261 group (ctrl IgG treated) is shown (left). The frequency of IFN- γ among CD45.2⁺ CD8⁺ TILs of mice with different tumor are shown. (B-C) one-way ANOVA analysis. (D-F) two-tailed student *t*-test analysis. **p* < 0.05, ***p* < 0.01,

Kumar et al.

*** $p < 0.001$, **** $p < 0.0001$, data represent the means \pm SEM of five mice. Data are representative of two independent experiments.

Figure 2: PD-1 blockade significantly enhances mitochondrial activity in CD8⁺ T cells in mice with responsive, but not in mice with unresponsive tumors.

(A) DLN CD8⁺ T cells were purified from pool of five mice per each group from the experiment of Figure 1. OCR of DLN CD8⁺ T cells was measured from responsive and unresponsive tumor groups (left). Other parameters associated with OCR graph (basal respiration, maximal respiration, spare respiratory capacity and ATP turnover) were calculated and values are plotted in bar graph for respective tumor group (right). Data represent the means \pm SEM of five wells. * $p < 0.05$, ** $p < 0.01$, *** $p < 0.001$, two-tailed student *t*-test analysis. (B-C) Tumor mass cells, from the experiment groups of Figure 1, were stained with anti-CD8, anti-CD45.2 antibodies and mitochondrial dyes for Mitochondrial Superoxide production (B) or Cellular ROS production (C). Representative histogram (left) and MFI (right) of mitochondrial dyes after gating on CD8⁺ T cells are shown. Data represent the means \pm SEM of five mice. * $p < 0.05$, ** $p < 0.01$, *** $p < 0.001$, one-way ANOVA analysis. Data are representative of two independent experiments (A-C).

Figure 3: Unresponsive tumors can be classified into systemically immunosuppressive or non-immunosuppressive tumors. (A) Unresponsive tumor cells (LLC, Pan02 and B16) were inoculated on left flank of C57BL/6N mice. On day 6, responsive tumor (MC38) cells were inoculated on the right flank of the same mice. On day 8, anti-PD-L1 mAb (or isotype control Rat IgG2a) was injected every fifth day thereafter. (B) Tumor growth of responsive MC38 on the right side was compared with or

Kumar et al.

without PD-1 blockade treatment. (C) Following the same schedule as mentioned in A, unresponsive tumor (CT26) cells and responsive tumor (MethA) cells were injected in BALB/c mice. Tumor growth of MethA on right side was shown. (B–C) Data represent the means \pm SEM of five mice. Data are representative of two independent experiments.

Figure 4: Unresponsive tumor-derived immune suppressive factor inhibits the mitochondrial responses in CD8⁺ T cells *in vivo*. (A) Mice were treated in the same way as Figure 3A and sacrificed on day 14 for the analysis of DLN CD8⁺ T cells. (B) Absolute number of lymphocytes per LN from MC38 side were calculated. (C) DLN cells harvested from MC38 side were stained with anti-CD8 mAb, MitoSox (left panels) and MitoMass (right panels). Representative FACS profiles after gating on CD8⁺ T cells and MFI of dye staining are shown. (D) OCR of CD8⁺ T cells purified from pooled DLN cells of MC38 side for different groups is shown (top). Basal respiration and ATP turnover values were calculated from OCR graph (bottom). (E) DLN cells harvested from unresponsive side were stained with anti-CD8 mAb, MitoSox (left) and MitoMass (right). Representative FACS profiles of DLN CD8⁺ T cells and the MFI of dye staining are shown. (F) OCR of CD8⁺ T cells purified from pooled DLN cells of B16 or LLC side is shown (left). Basal respiration and ATP turnover values were calculated from OCR graph (right). (B, C, E) Data represent the means \pm SEM of five mice. $*p < 0.05$, $**p < 0.01$, two-tailed student *t*-test analysis. (D,F) Data represent the means \pm SEM of five wells. $*p < 0.05$, $**p < 0.01$, one-way ANOVA analysis. Data are representative of two independent experiments.

Figure 5: The absence of MHC class I expression in B16. (A-B) Tumor growth of responsive and unresponsive tumors were observed in wild type or immune-compromised

Kumar et al.

(Rag2^{-/-}) mice. Tumor sizes of responsive tumors (A) and unresponsive tumor (B) are shown. Data represent the means \pm SEM of 5 mice. (C-D) Responsive and unresponsive tumor cells were stimulated with IFN- γ for overnight, followed by staining with anti-H-2Kb/H-2Kd mAbs. Representative histograms of MHC class I for responsive (C) and unresponsive (D) tumor cells are shown. Data represent the means \pm SEM of three wells. Data are representative of three independent experiments.

Figure 6: Small soluble factors released from SIP-positive tumors inhibits the T cell proliferation and mitochondrial function *in vitro*. (A) Naïve CD8⁺ T cells (CD44⁺ CD8⁺ T cells) were purified from spleen and LNs of C57BL/6N mice. Naïve CD8⁺ T cells were stimulated with anti-(CD3+CD28) mAbs-coated dynabeads for 48 hours with or without culture supernatant from different tumor cell lines. (B) T-cell proliferation was measured by ³H-thymidine incorporation assays. (C) T cells were stained with anti-CD8 mAb, CellRox (cellular ROS, left) and MitoTracker Deep Red (mitochondrial potential, right) after the stimulation. The MFI of mitochondrial dyes of CD8⁺ T cells are shown. (D-E) OCR (D) and ECAR (E) of T cells were measured. The OCR graph without (left) or with culture supernatants groups (right) are shown. (F) LLC supernatant was heat-inactivated to denature protein components. To remove small molecules, supernatant was treated with dextran-coated charcoal (DCC) that adsorbs small molecules. The effects of treated supernatant on T cell proliferation was assessed. (G) Using different cut-off filters, LLC supernatant was fractionated into <3kDa and <50kDa fractions that were further treated with DCC. The effects of the treated fractions on naïve CD8⁺ T cell proliferation was assessed. Data represent the means \pm SEM of three wells. **p* < 0.05, ***p* < 0.01,

Kumar et al.

*** $p < 0.001$, **** $p < 0.0001$, one-way ANOVA analysis (B-G). Data are representative of three independent experiments.

Figure 7: Enhancing mitochondrial activation by bezafibrate partially overcomes suppression and improves survival of SIP-positive tumor-bearing hosts *in vivo*.

(A) Naïve CD8⁺ T cells purified from spleen and LNs of C57BL/6N mice were stimulated for 48 hours with anti-(CD3+CD28) mAb along with LLC culture supernatant and Bezafibrate (5μM). Following incubation, OCR of T cells was measured. Data represent the means ± SEM of three wells. * $p < 0.05$, ** $p < 0.01$, *** $p < 0.001$, one-way ANOVA analysis. (B) Unresponsive tumors (B16 and LLC) were injected and the mice were treated with anti-PD-L1 mAb along with Bezafibrate (5mg/kg). Schematic diagram of the combination therapy schedule. (C) Tumor graph (left) and survival curve (right) are shown for the B16 (upper panel) and LLC (lower panel) tumor-bearing host treated with Bezafibrate combination therapy. Data represent the means ± SEM of five mice (C-D). * $p < 0.05$, one-way ANOVA analysis. Data are representative of three independent experiments (A-C).

Kumar et al.

746 **Table 1. Mechanistic classification of unresponsive tumors.**

Background	Name of tumor	Releasing suppressive factor (related to fig. 3)	Activation of acquired immunity (related to fig. 5)
C57BL/6N	B16	No	No
	LLC	Yes	Less
	Pan02	Yes	No
BALB/c	CT26	Yes	Less

747

Figure 1.

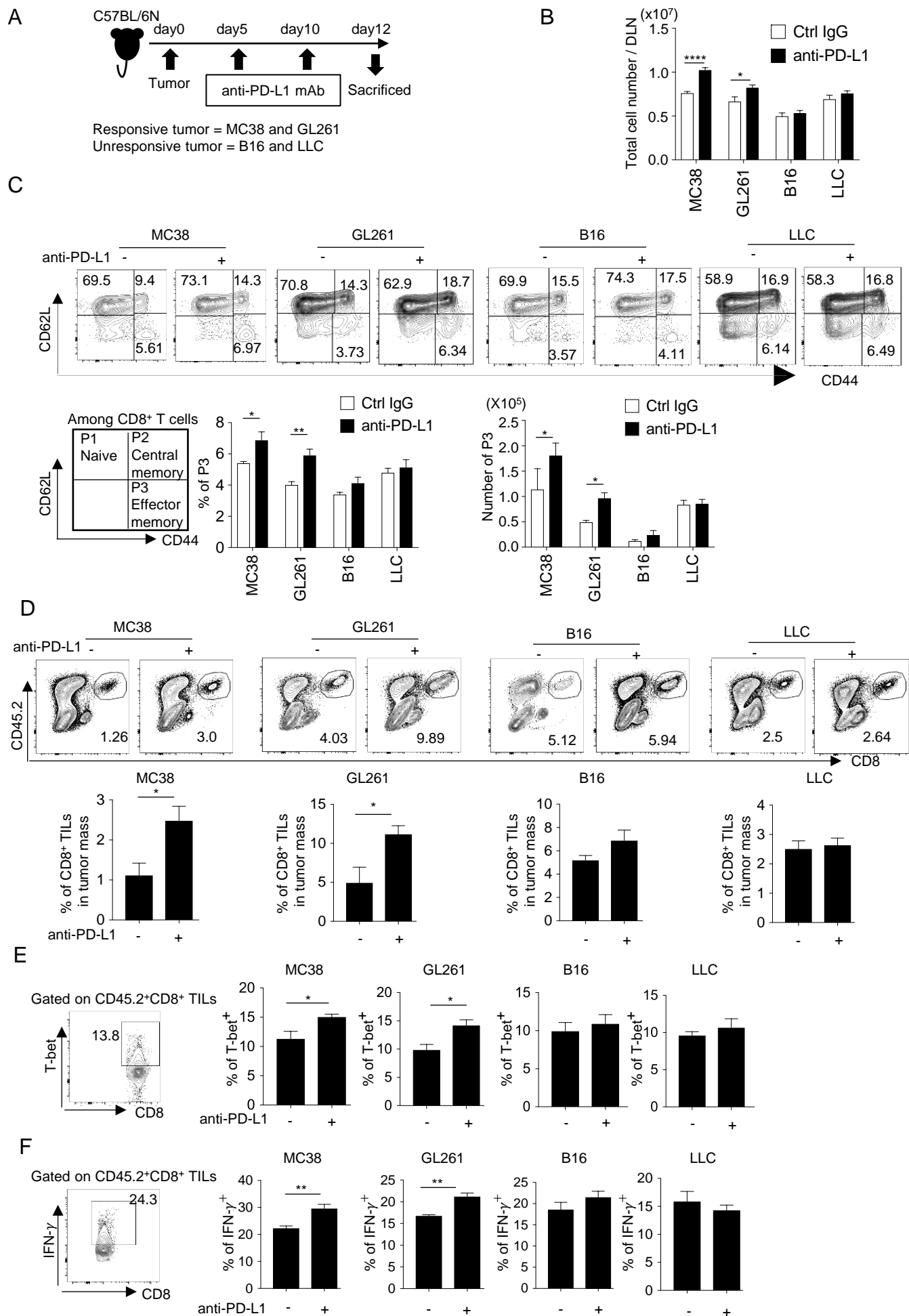


Figure 2.

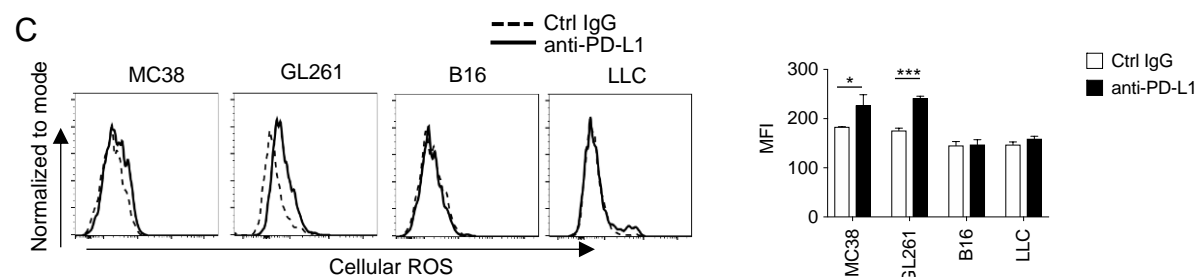
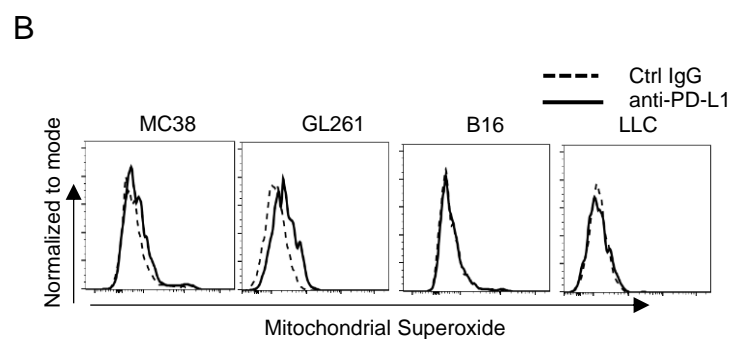
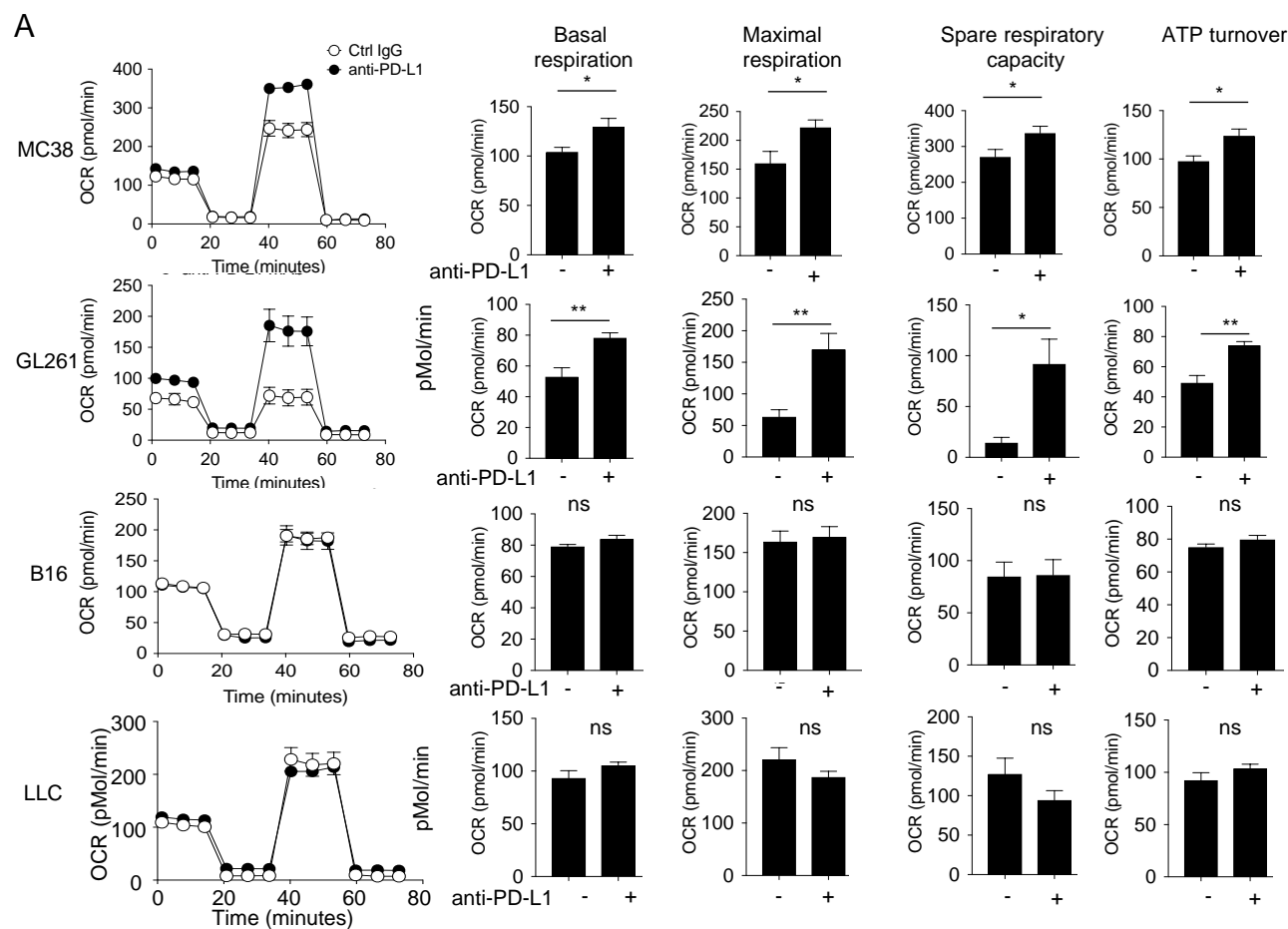


Figure 3.

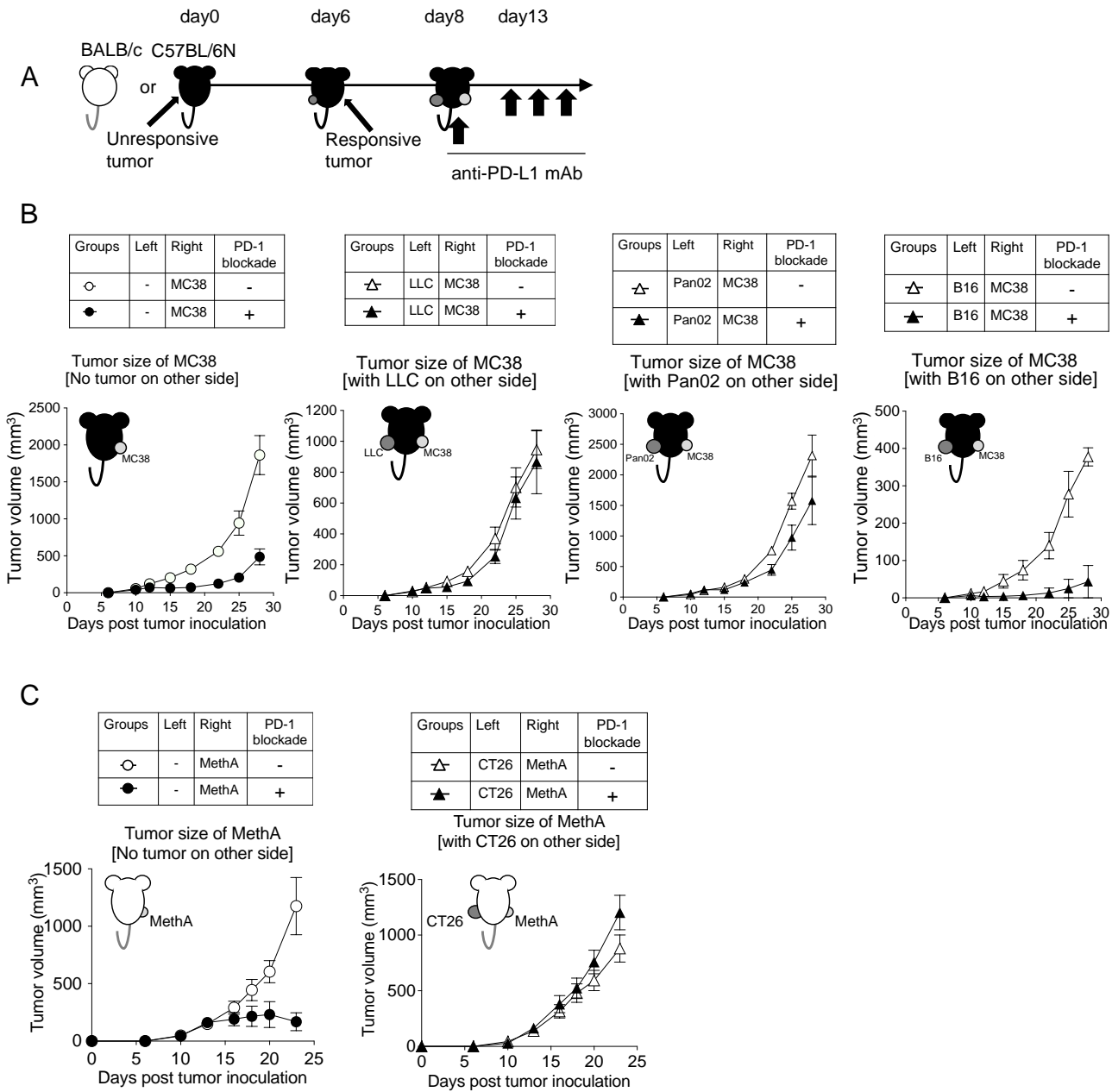


Figure 4.

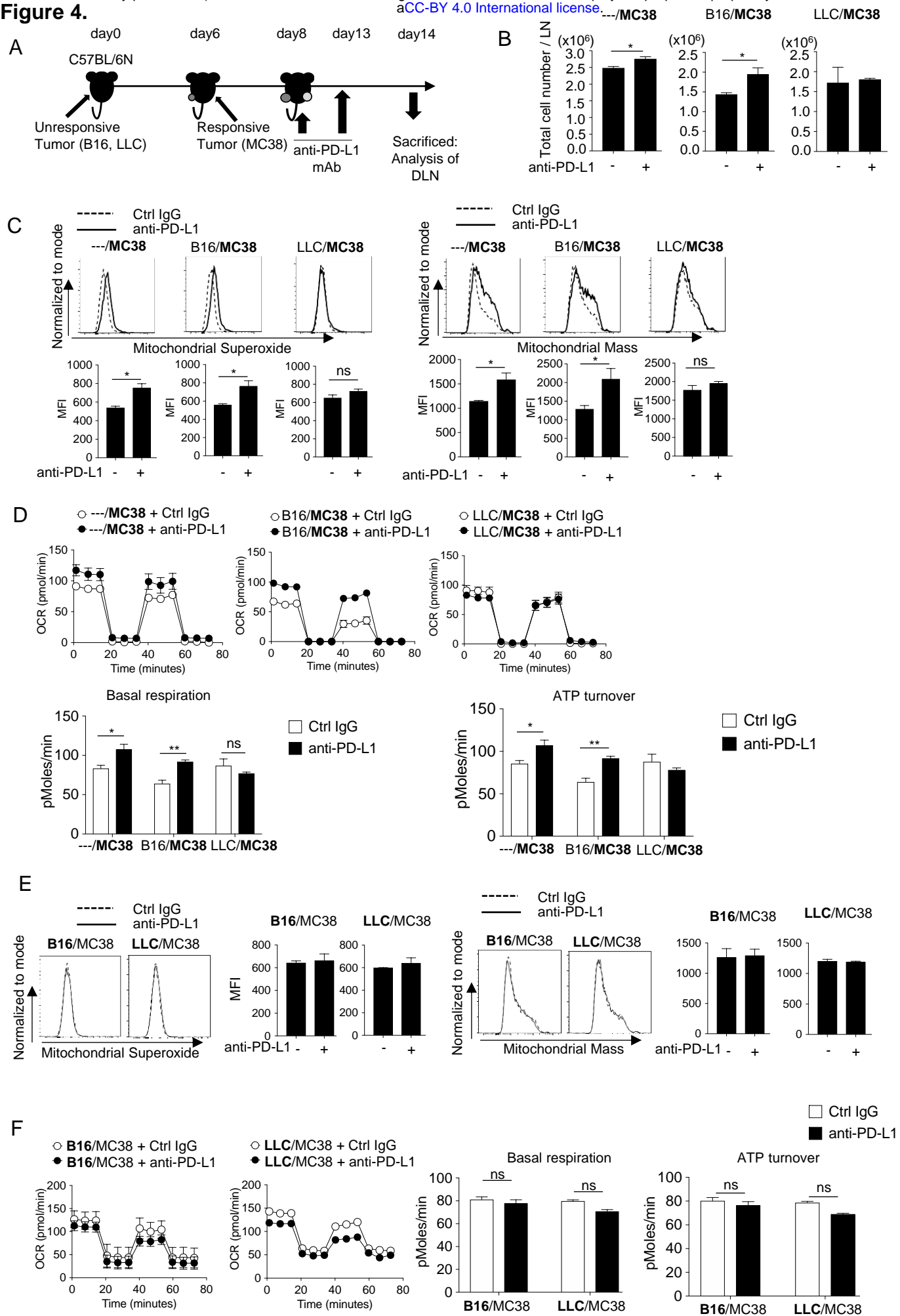


Figure 5.

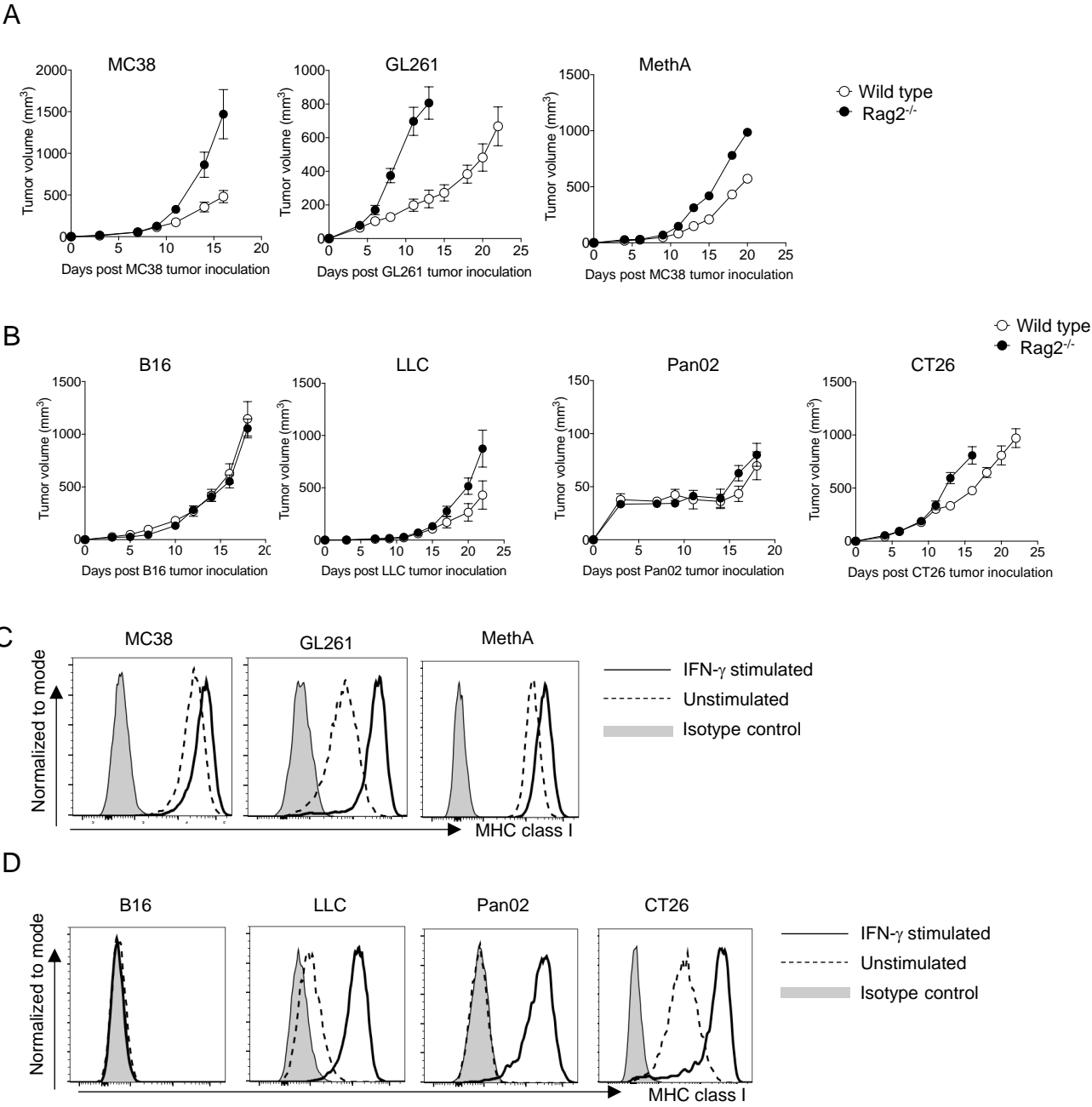


Figure 6.

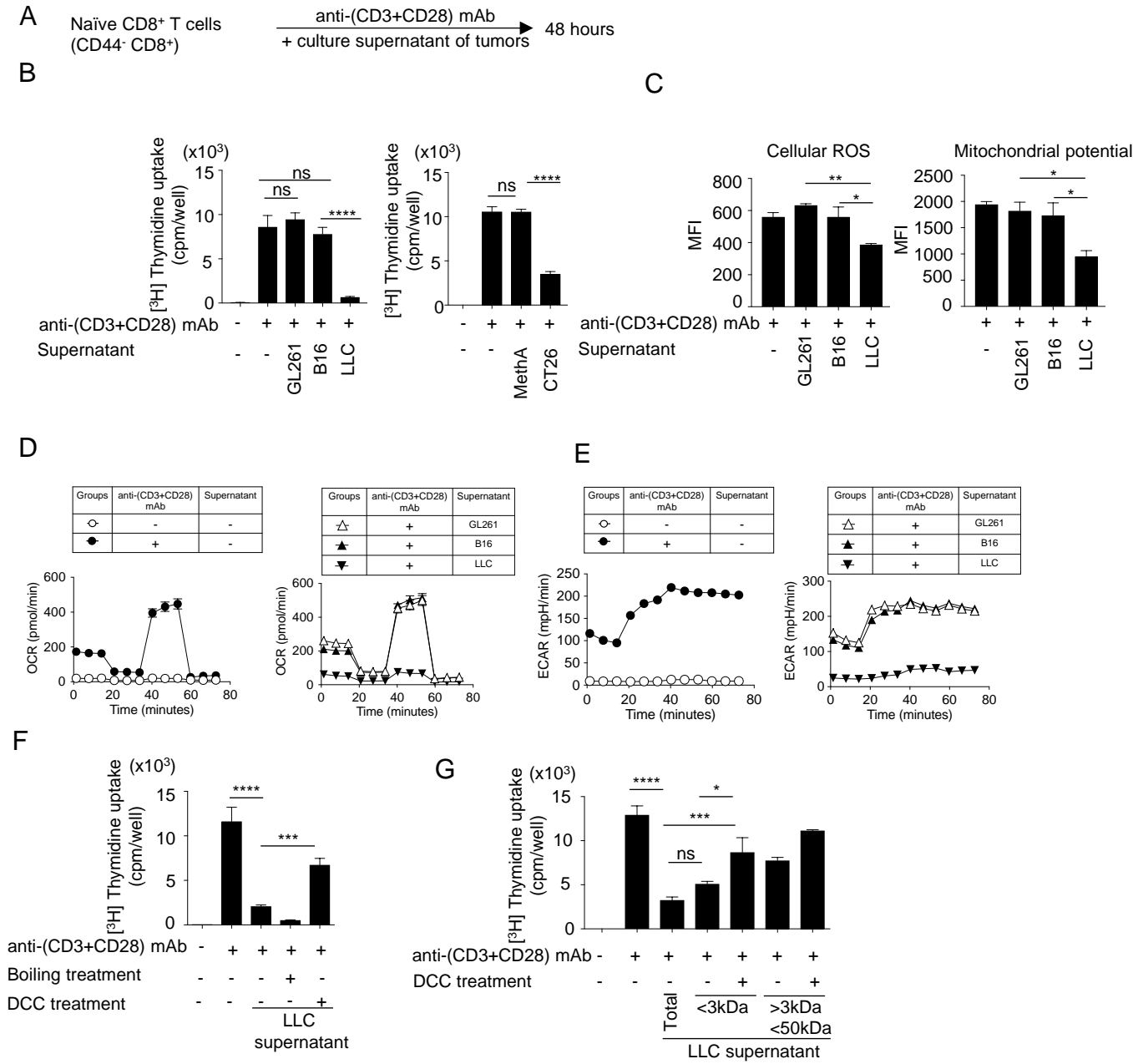
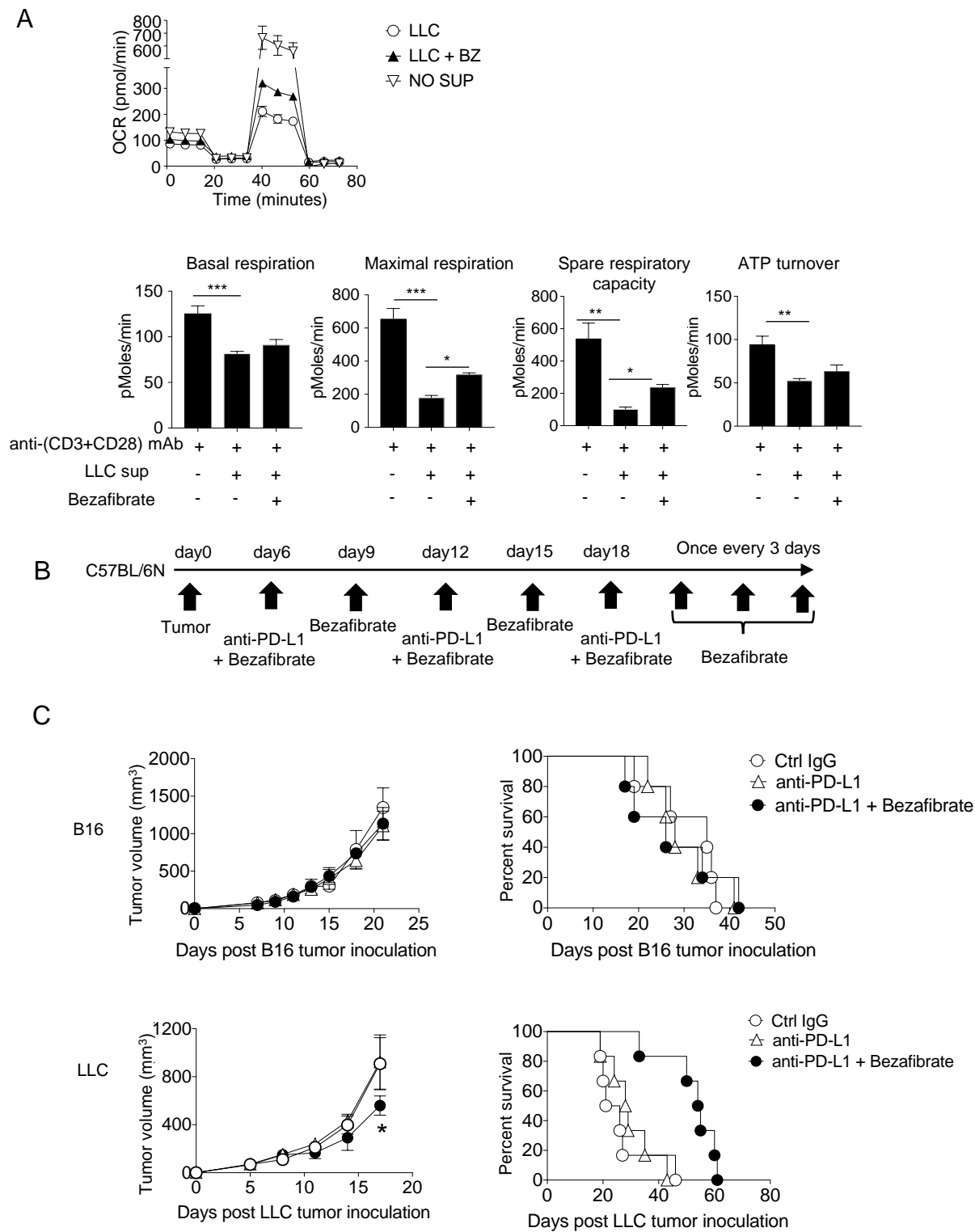
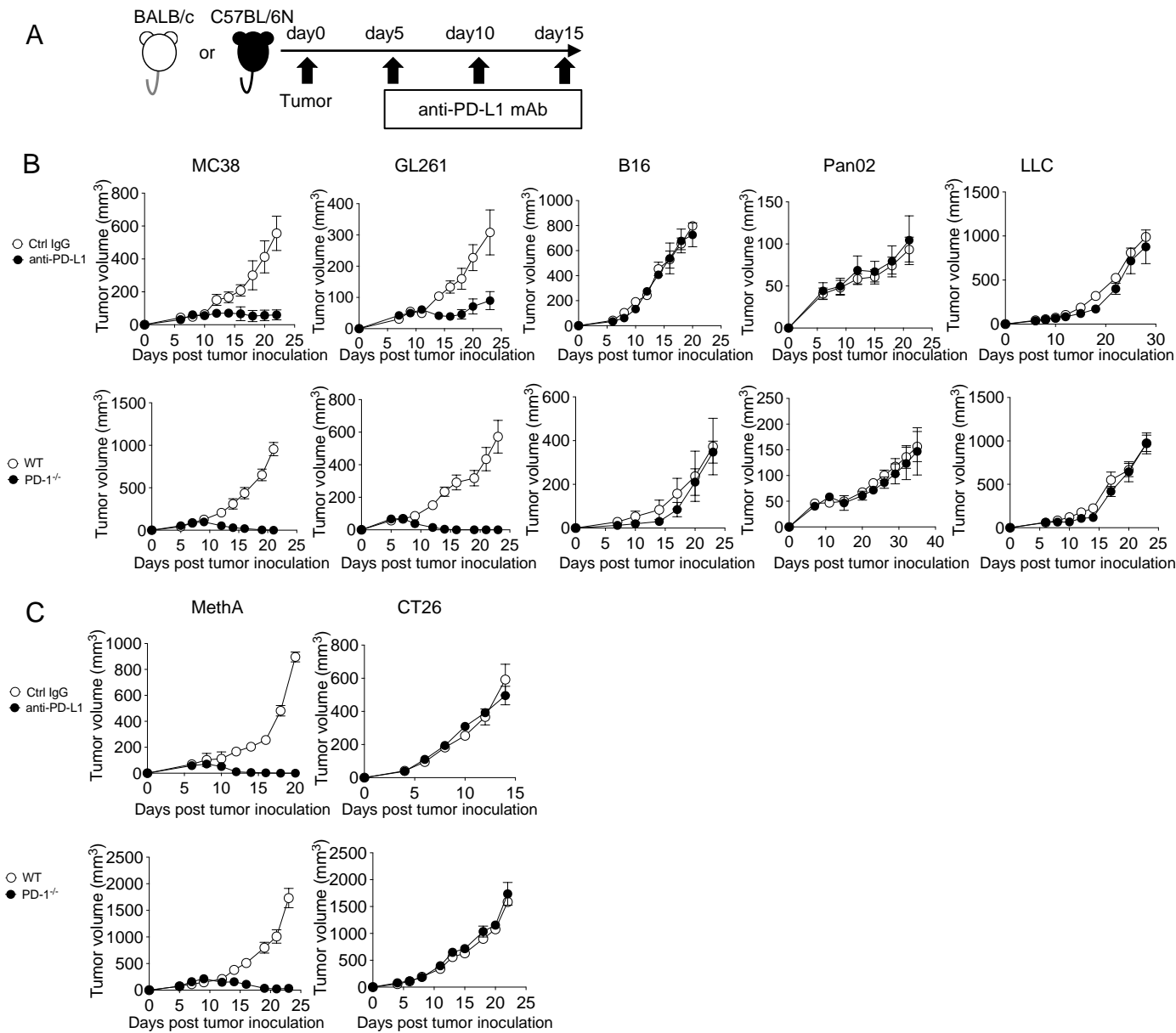


Figure 7.



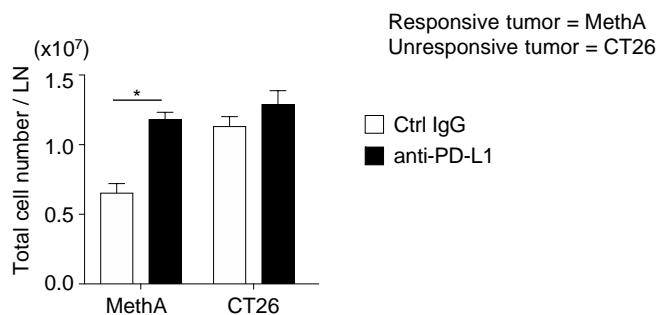
Supplementary Figure S1



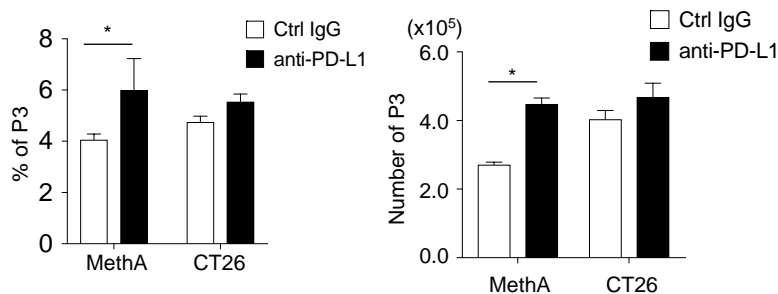
Supplementary Figure S1. Stratification of responsive and unresponsive tumors in C57BL/6N and BALB/c genetic backgrounds. (A) Schematic diagram of the PD-1 blockade therapy. Tumor size was measured on every alternative day. (B-C) Tumor growth were measured in anti-PD-L1 mAb treatment model (top panel) or genomic PD-1^{-/-} model (bottom panel) in C57BL/6N (B) and BALB/c (C) background. Data represent the means \pm SEM of five or six mice. Data are representative of three independent experiments.

Supplementary Figure S2

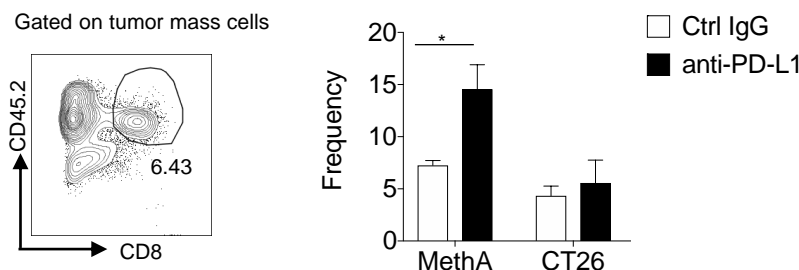
A



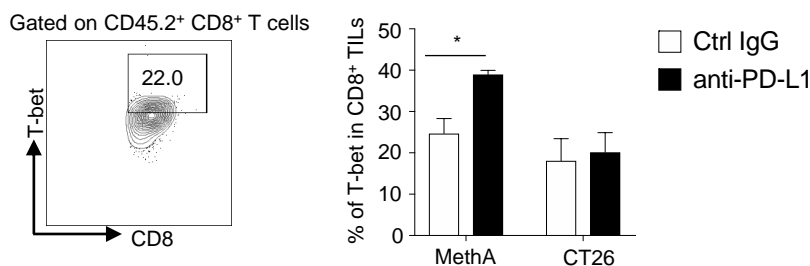
B



C



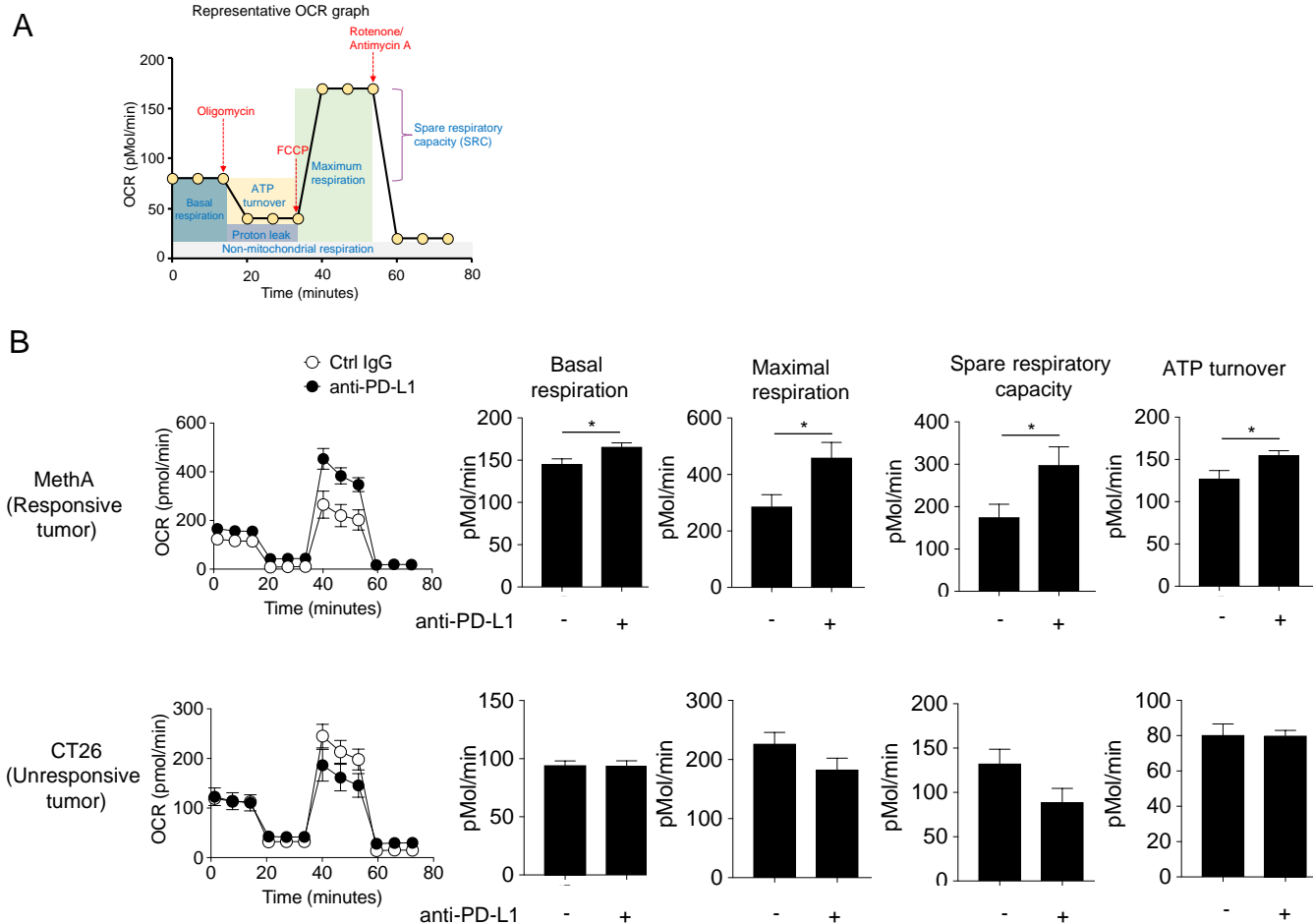
D



Supplementary Figure S2. Higher immune responses in responsive tumor-bearing host after PD-1 blockade than to unresponsive group in BALB/c background.

Following the experimental schedule as mentioned in Figure 1A, mice were sacrificed on day 12 for analysis of immune responses. (A) Absolute number of lymphocytes per LN were compared between responsive and unresponsive tumor-bearing hosts. (B) DLN cells were stained with anti-CD8, anti-CD62L, and anti-CD44 antibodies. Frequency (left) and absolute number (right) of effector memory CD8⁺ T cells (P3 population) were calculated. (C-D) Cells after tumor digestion were stained with anti-CD8 and anti-CD45.2 mAb. Representative FACS pattern of CD45.2⁺ CD8⁺ CTLs from MethA-bearing mice treated with ctrl IgG group is shown (left). The frequency of CD45.2⁺ CD8⁺ CTLs was compared between responsive and unresponsive tumor-bearing hosts (right) (C). Following surface staining, T-bet was stained intranuclearly. Representative FACS pattern from MethA-bearing mice treated with ctrl IgG group (left) and the bar graph of frequency of T-bet expression are shown (right) (D). Data represent the means \pm SEM of five or six mice. * $P < 0.05$, one-way ANOVA analysis. Data are representative of two independent experiments.

Supplementary Figure S3



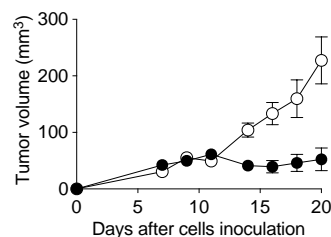
Supplementary Figure S3. CD8⁺ T cells from mice with sensitive tumor have higher mitochondrial activity after PD-1 blockade than those with unresponsive tumors in BALB/c background. (A) Representative OCR plot by Seahorse XF^e analyzer, showing basal respiration, maximal respiration, spare respiratory capacity, ATP turnover, proton-leak, and non-mitochondrial respiration, is shown. (B) OCR of DLN CD8⁺ T cells was measured from experimental groups of supplementary figure S2. DLN CD8⁺ T cells were purified from pooled cells of each group. OCR plot (left) and its associated parameters (right) from responsive tumor (top panels) and unresponsive tumor (bottom panels) are shown. Data represent the means \pm SEM of five wells. * $P < 0.05$, two-tailed student t-test analysis. Data are representative of two independent experiments.

Supplementary Figure S4

A

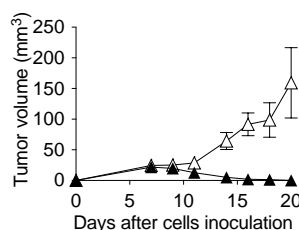
Groups	Left	Right	PD-1 blockade
○	-	GL261	-
●	-	GL261	+

Tumor size of GL261
[no tumor on other side]



Groups	Left	Right	PD-1 blockade
△	B16	GL261	-
▲	B16	GL261	+

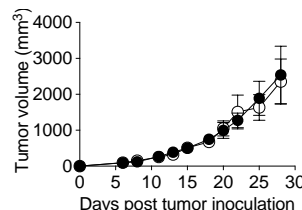
Tumor size of GL261
[with B16 on other side]



B

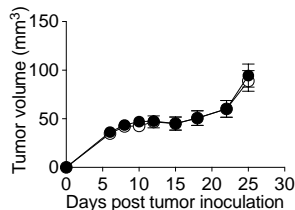
Groups	Left	Right	PD-1 blockade
○	LLC	MC38	-
●	LLC	MC38	+

Tumor size of left tumor (LLC)



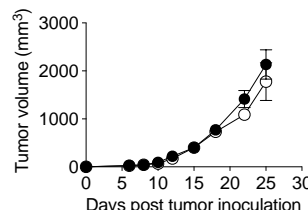
Groups	Left	Right	PD-1 blockade
○	Pan02	MC38	-
●	Pan02	MC38	+

Tumor size of left tumor (Pan02)



Groups	Left	Right	PD-1 blockade
○	B16	MC38	-
●	B16	MC38	+

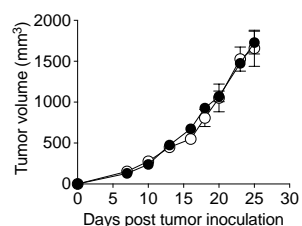
Tumor size of left tumor (B16)



C

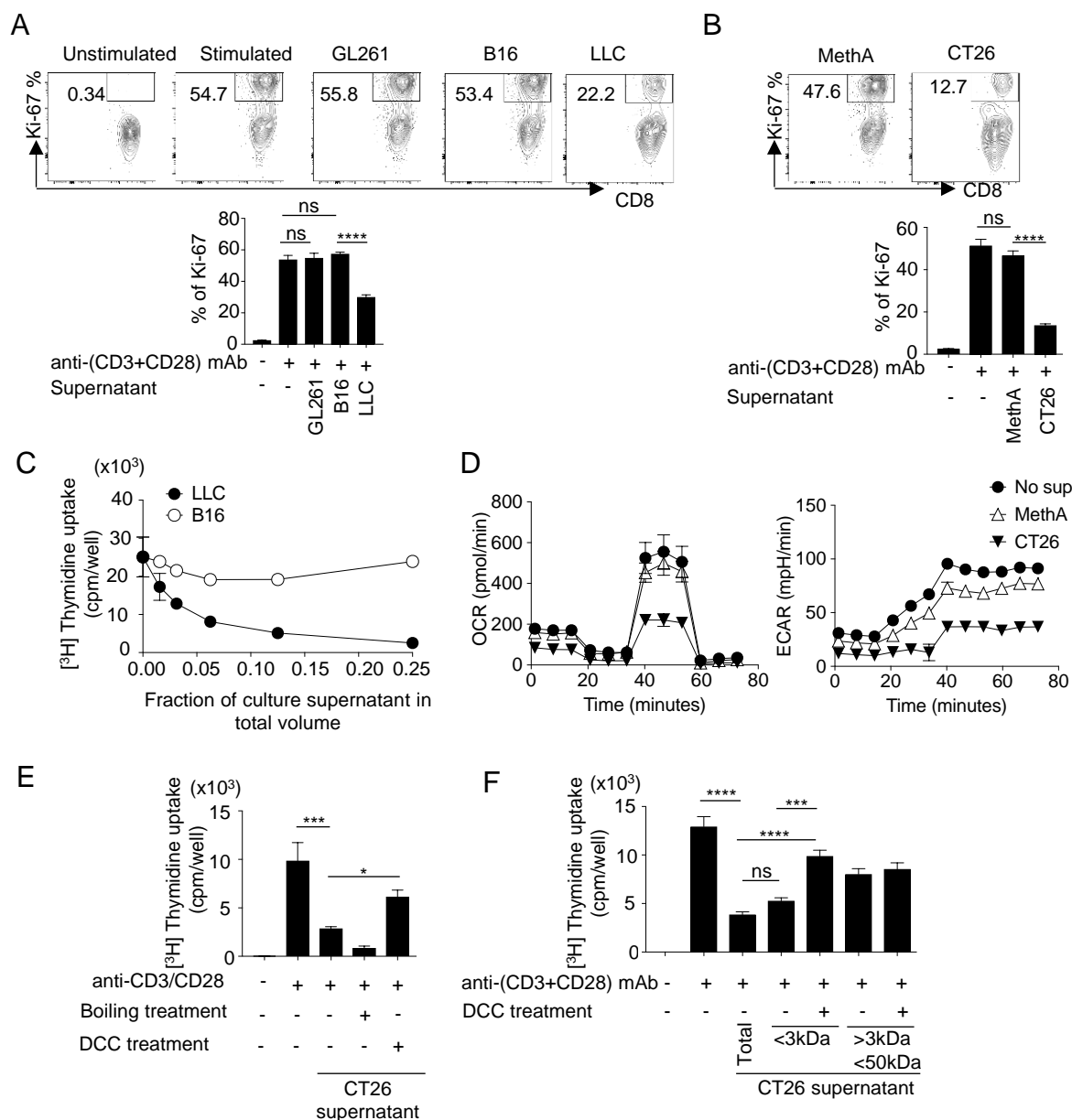
Groups	Left	Right	PD-1 blockade
○	CT26	MethA	-
●	CT26	MethA	+

Tumor size of left tumor (CT26)



Supplementary Figure S4. Unresponsive tumors can be classified into systemically immunosuppressive or non-immunosuppressive tumors. (A) Unresponsive tumor (B16) and responsive tumor (GL261) were injected and therapy were given as per the schedule mentioned in Figure 3A. Tumor growth of right responsive tumor (GL261) with or without PD-1 blockade was compared when no tumor (left panel) or in the presence of B16 (right panel) on left side. (B and C) Unresponsive tumor growth on left side of Figure 3B or C are shown. Data represent the means \pm SEM of five mice. Data are representative of two independent experiments.

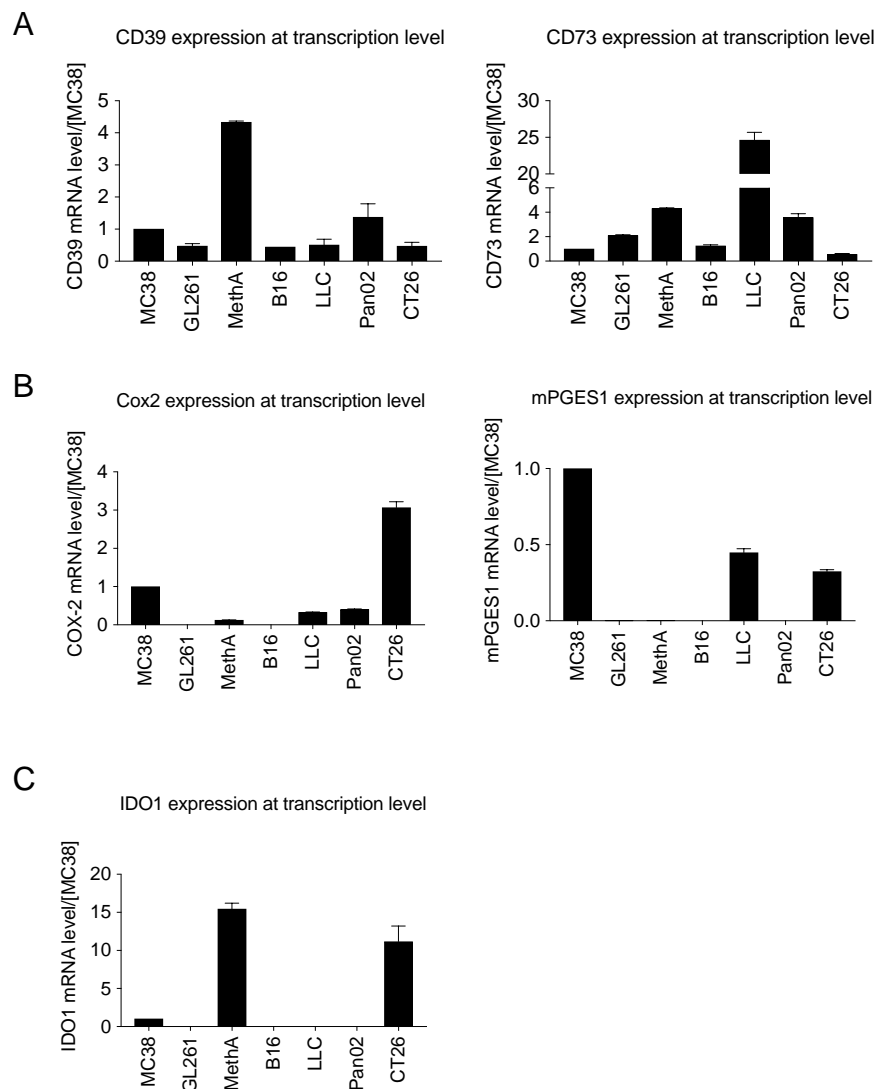
Supplementary Figure S5



Supplementary Figure S5. Tumor-derived suppressive factor inhibits proliferation and mitochondrial function of CD8⁺ T cells *in vitro*.

As per schedule mentioned in Figure 6A, naïve CD8⁺ T cells were stimulated in the presence of culture supernatant. (A-B) Naïve CD8⁺ T cells were stimulated in the presence of culture supernatant of tumor cells from C57BL/6N (A) or BALB/c (B) background. Ki-67 expression was analyzed intracellularly by flow cytometry. Representative FACS profile (upper panel) and frequency of CD8⁺ KI-67⁺ T cells (lower panel) are shown. Control groups are shared between A and B. (C) Naïve CD8⁺ T cells were stimulated in the presence of serially diluted culture supernatants from B16 and LLC. T cell proliferation was measured by ³H-thymidine incorporation assay. (D) OCR (left) and ECAR (right) were measured of naïve CD8⁺ T cells that were stimulated in the presence of culture supernatant from MethA and CT26. (E) CT26 supernatant was heat-inactivated to denature protein components. To remove small molecules, supernatant was treated with DCC. The effect of treated supernatant on naïve CD8⁺ T cell proliferation was assessed. (F) Using different cut-off filters, CT26 supernatant was fractionated into <3kDa and <50kDa fraction that were further treated with DCC. The effect of treated fractions on naïve CD8⁺ T cell proliferation was assessed. Data represent the means ± SEM of triplicate wells. **p* < 0.05, ***p* < 0.01, ****p* < 0.001, *****p* < 0.0001, one-way ANOVA analysis. Data are representative of three independent experiments.

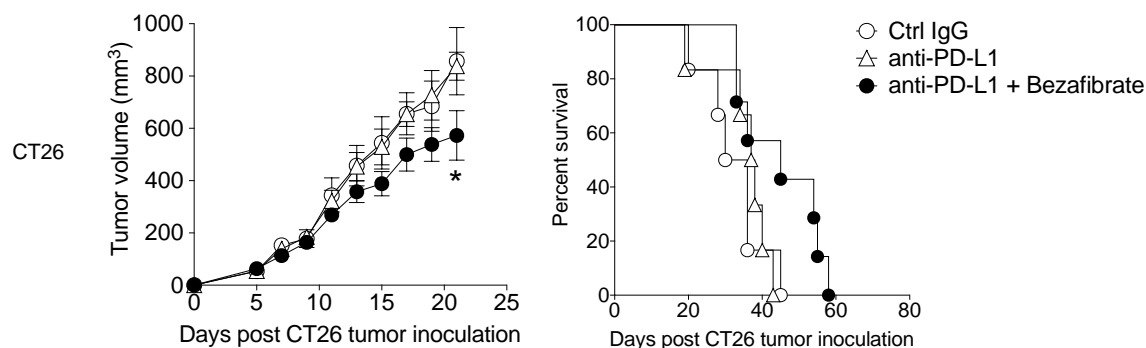
Supplementary Figure S6



Supplementary Figure S6. The systemic immunosuppressive factors are uncharacterized.

Expression levels of immune suppression-associated genes were examined by quantitative PCR (qPCR) in different tumor cell lines. **(A)** Expression of CD39 (left) and CD73 (right) were quantified. **(B)** Expression of Cox2 (left) and mPGES1 (right) were quantified. **(C)** Expression of IDO1 was quantified. Data represent the means \pm SEM of 3 wells assuming the expression in MC38 = 1 in qPCR analysis. Data are representative of 3 independent experiments.

Supplementary Figure S7



Supplementary Figure S7. Enhancing mitochondrial activation by bezafibrate chemicals improves the anti-tumor effect for SIP-positive tumor in BALB/c background. SIP-positive CT26 tumor was injected in mice and therapy was given as per schedule mentioned in Figure 7B. Tumor size (left) and survival (right) of CT26 tumor-bearing host are shown. Data represent the means \pm SEM of five mice. * $p < 0.05$, one-way ANOVA analysis. Data are representative of three independent experiments.

Supplementary Table S1. List of mouse cell lines from different genetic backgrounds used in this study.

Cell line	Background	Response to PD-1 blockade therapy	Particulars	Source
GL261	C57BL/6N	Responsive	Glioblastoma cell line	As a gift from Kyushu University, Kyushu, Japan
MC38	C57BL/6N	Responsive	Colon carcinoma cell line	As a gift from Dr. James P. Allison, Memorial Sloan-Kettering Cancer Center (New York, NY, USA)
LLC	C57BL/6N	Unresponsive	Lewis lung carcinoma cell line	American Type Culture Collection
B16	C57BL/6N	Unresponsive	Melanoma cell line	As a gift from Dr. Nagahiro Minato, Graduate School of Medicine, Kyoto University
Pan02	C57BL/6N	Unresponsive	Pancreatic ductal adenocarcinoma cell line	National Cancer Institute
MethA	BALB/c	Responsive	3-methylcholanthrene (MCA)-induced fibrosarcoma cell line	Cell Resource Center for Biomedical Research (Sendai, Japan)
CT26	BALB/c	Unresponsive	N-nitroso-N-methylurethane-(NNMU) induced colon carcinoma cell line	National Cancer Institute

Supplementary Table S2. List of primers for quantifying mouse gene transcripts by RT-qPCR.

Transcript	Forward primer	Reverse primer
CD39	TACCACCCCATCTGGTCATT	GGACGTTTTGTTTGTTGGT
CD73	CAAATCCCACACAACCACTG	TGCTCACTTGGTCACAGGAC
COX2	CAAGGGAGTCTGGAACATTG	ACCCAGGTCCTCGCTTATGA
mPGES1	ATGAGTACACGAAGCCGAGG	CCAGTATTACAGGAGTGACCCAG
IDO1	CACTGAGCACGGACGGACTGAGA	TCCAATGCTTTCAGGTCTTGACGC
β-actin	TATTGGCAACGAGCGGTTCC	GGCATAGAGGTCTTTACGGATGT